ABSTRACT

NUMERICAL INVESTIGATIONS OF A PIPE JET WITH COIL INSERT ISSUING INTO A CROSSFLOW

BY

Saul Guzman

January 2015

Numerical investigations of a jet in crossflow with two different coil inserts at four ratios of jet to the crossflow mean velocities were performed. The coils had a length to diameter (L/D) ratios of 2 and 11.25 and the velocity ratios, r, were 0.5, 1.0, 2.0, and 5.0. Results show when r=0.5, with coil inserts, jet penetration into the crossflow is reduced with increased entrainment near the jet outlet. Further results show that when r=2, and 5, near the jet outlet entrainments are reduced, with jet penetrating into higher elevations, before tilting in the direction of the crossflow. Comparing the results for the two coil inserts, with the shorter coil insert, higher penetration is obtained and with the longer coil, turbulent kinetic energy is increased in the near field.

NUMERICAL INVESTIGATIONS OF A PIPE JET WITH COIL INSERT ISSUING INTO A CROSSFLOW

A THESIS

Presented to Department of Mechanical and Aerospace Engineering

California State University, Long Beach

In Partial Fulfillment

of the Requirements for the Degree

Master of Science in Mechanical Engineering

Committee Members:

Hamid R. Rahai, Ph.D. (Chair)
Praveen Shankar, Ph.D.
Huy T. Hoang, Ph.D.

College Designee:

Antonella Sciortino, Ph.D.

By Saul Guzman

B.S., 2012, California State Polytechnic University, Pomona

January 2015

ACKNOWLEDGEMENTS

I would like to recognize the many individuals for sharing their knowledge and helping complete this thesis. I am grateful for the insight they provided me and thankful for I would not be in the position I am in my educational career without them.

First and foremost, I would like to express my profound gratitude to Dr. Hamid R. Rahai for serving as my advisor and mentor. For sharing his knowledge with me in the classroom and out, for making himself available to answer my questions and having the patience to make sure I left with a clear understanding throughout this process.

I would like to express my gratitude to Dr. Praveen Shankar and Dr. Huy T. Hoang for serving as the committee members on the thesis panel.

I would like to thank my friends and peers for their support and encouragement. My family for supporting me in my educational endeavors and their constant motivation to pursue my educational goals for I am forever grateful and will never forget.

Lastly, I would like to thank my girlfriend, Yazmin Mendoza, for her constant support, motivation, and patience throughout my educational career. Without her help I would not be able to complete this report.

TABLE OF CONTENTS

Page

CHAPTER Page

LIST OF TABLES

TABLE Page

LIST OF FIGURES

FIGURE Page

FIGURE Page

FIGURE Page

FIGURE Page

ABBREVIATIONS

D	Jet diameter
Re_D	Reynolds Number, $\frac{U_j D}{\nu}$
Re_L	Reynolds Number, $\frac{U_j L}{\nu}$
d	Coil Diameter
TKE	Turbulent Kinetic Energy
L	Length of Coil
r	Velocity Ratio, $\frac{U_j}{U_e}$
U_e	Crossflow Velocity
U_j	Jet Inlet Velocity
U_m	Jet Mean Outlet Velocity
P	Pitch of Coil
s	Swirl Number, $\frac{G_\theta}{(\frac{D}{2})G_x}$
G_x	Axial Flux of Axial Momentum
G_θ	Axial Flux of Angular Momentum
W	Counter rotating pair width
x	Position in the x-direction along surface
y	Position in the y-direction

CHAPTER 1

INTRODUCTION

Jet in cross-flow (JICF) arises from turbulent jets injected into a crossflow, where its mixing field is widely studied for various applications. Industrial applications of jet in crossflow include fuel injection, cooling of turbine blades, and dilution holes in gas turbine combustors. In the case of fuel injection, better understanding of JICF had lead to better efficiency and reduced emissions. Dilution holes in gas turbine combustors are used to cool the flow before it reaches the turbine stages where as the turbine blades are cooled through the injection of cool air, adding a protective layer to ensure durability. In the field of air pollution, the conventional smoke stacks found in most power plants can carry hazardous material in their exhaust, therefore better mixing with the crossflow is needed to disperse pollution and reduce their local concentrations.

Previous works have focused on a jet emerging from a flat surface [1, 2]. As the jet enters the crossflow, it is deflected in the direction of the crossflow as shown in Figure 1. The dominate feature is the counter rotating vortex pair (CVP) that assumes a symmetrical kidney shape structure, that is created in near field through the distortion of the jet vortices in the jet shear layer. Horseshoe vortices are formed in the plane and surround the exiting jet. Lastly, there are wake vertices created that run from the plane to the CVP. It has been suggested that wake vertices carry fluid from the boundary layer to the CVP [3].

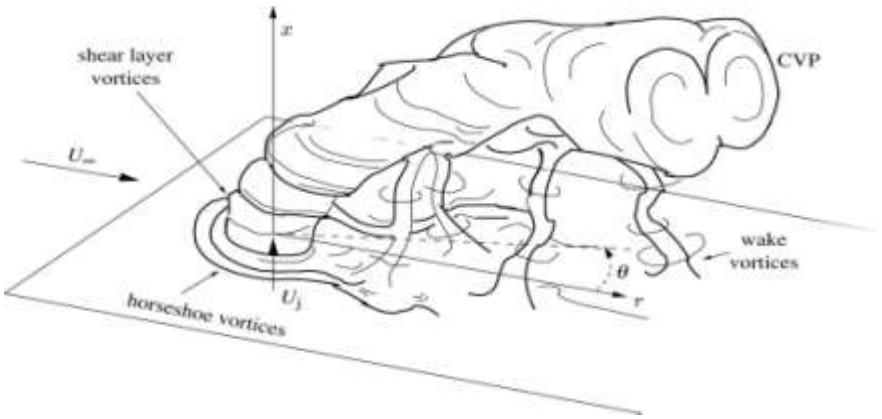

FIGURE 1. Schematic of the transverse jet [3].

The objectives of the present investigations were to examine mixing enhancement and control jet penetration, using coil inserts. CD-Adapco's computational fluid dynamics program, Star CCM+, was used for the numerical investigations. Results include contours of the mean velocity, mean pressure, vorticity, and turbulent kinetic energy at various planes perpendicular to the crossflow at and downstream of the jet. In addition, trajectory of the jet with and without the coil inserts were computed from the locations of maximum axial mean velocity and compared for assessment of jets' penetrations and mixing. Lastly, the widths of the CVP were compared with and without coil inserts to determine the crossflow entrainment on the jet.

1.1 Review of Literature

1.1.1 Flushed Jet

The CVP is considered as the trademark of a JICF and it is symmetric instantaneously as the jet interacts with the crossflow. The original jet disappears as the jet bends and a pair of vortices dominate the flow field.

The jet shear-layer vortices shown in Figure 1, which dominate the initial portion of the jet, are a result of the Kelvin-Helmholtz instability of the annular shear layer that

separates from the edge of the jet orifice [3]. CVP formation is delayed as the jet velocity ratio increases such as in Smith and Mungal's [2] experiments where they found that CVP formation was slower at r = 20 as compared with r = 10, based on the distances from the jet exit normalized with rd, where r is the velocity ratio and d is the jet diameter.

Horseshoe vortices seen at the jet exit are formed when the jet is injected flushed within the bottom wall and evolve from the interaction of the jet with boundary layer. Andreopoulos and Rodi [1] suggests that the horseshoe vortices arise from vortex line being deflected around the jet, similar to a boundary layer when it is deflected around an obstacle.

Wake vortices are known to exist downstream from the jet exit beneath the CVP. Wake vortices contain a complex system of vortices which are attached to the bottom wall and terminate on the CVP. They are the least understood characteristic but Fric and Roshko [3] suggest they may evolve from the boundary layer of the wall from which the jet is issued. Furthermore, they explain that the adverse pressure gradient imposed by the external flow causes eruptions in the boundary layer from which these vortices are created.

1.1.2 Elevated Jet

Few studies, such as Eiff,et al. [4] and Habli et al. [5], on JICF were made with an elevated stack. Many of the same characteristics are found on an elevated jet as those found in flushed emitting jets. The CVP is seen to develop due to shear layer vortices; Eiff et al. [4] and Habli et al. [5] both show the formation of CVP.

One distinct feature shown by Habli et al. [5] was that there are two horseshoe vortices present: one is at the jet exit and the other at the bottom of the pipe extrusion.

Additionally, they postulate that due to the two horseshoe vortices created, the formation of the vortices in the wake are fundamentally different from the well-known phenomenon of vortex shedding from solid bluff bodies that Eiff et al. [4] detailed creating of upright wake vortices formed with an elevated jet. It was stated that due to the elevated stack, there are two wake regions formed due to the jet and the stack. Furthermore, it was shown that there is vortex shedding from the jet wake and stack wake that can be both described as Karman-like vortices and they tend to "lock-in" and create the wake vortices. The jet vortex originates from inside the pipe where it is concentrated in the jet shear layer whereas the stack vorticity is generated by the stack boundary layer outside the stack.

1.1.3 Vortex Generator

Vortex generators have been studied widely for their use in increasing the mixing process in internal flow and the ability to delay local flow separation and aerodynamic stalling. Previous work from Almoukdad et al. [6] investigated the use of coil inserts to enhance mixing of a jet issuing into a still air. Their results showed that coil inserts enhance mixing in the near field. Additionally, they suggested that maximum mixing enhancement can be obtained with coil pitch spacing (p/D) and coil to pipe inside diameter (d/D) near 1.0 and 0.1 respectfully. Their further investigations showed that coil inserts with ratios of coil length to the pipe diameter (L/D) of about 11.26 and 22.5 create the largest mixing process at the pipe outlet or in the near field. Reducing the coil length to L/D=1.41 provides a higher mixing value downstream; therefore decreasing the L/D would delay the mixing process to a further downstream location.

1.1.4 Swirl Jets

Swirl jets have been studied with variety of applications that include turbo machinery as in jet engines and turbo-pumps. In combustion, it allows for flame stabilization and a more intense mixing of air and fuel. The efficiency of chemical reactors and mixing devices is enhanced by making use of the faster spreading and more rapid mixing of the swirled jet with its surrounding. An important parameter in swirl jets is the swirl number (s) defined as

$$s = \frac{G_\theta}{(\frac{D}{2})G_x} = \frac{\int \rho u_\theta u_x r dA}{(\frac{D}{2})\int \rho u_x^2 dA} \quad [1]$$

Swirl number can be controlled by changing the initial tangential velocity in swirl generators.

Feyedelem and Sarpkaya [7] performed investigations of swirl jets into free and near free surfaces. Experiments were performed in a recirculation free-surface water tunnel with an axial-plus-tangential-entry swirl generator. Results were measured with a 10-W coherent laser system. Swirl numbers varied from s=0 to s=0.522 where the critical swirl number was found to be s=0.50 and s=0.51. A swirl number of 0.522 corresponds to a strong swirl. Their results showed that at s=0.265 a gradual increase in velocity decay occurs and it is due to centrifugal expansion of the jet. At critical swirl numbers the velocity decreases rapidly to zero and picks back up to 30% of the axial mean velocity. Axial velocity reverses and vortex breakdown occurs at the jets core at swirl number equal to 0.522. Turbulent kinetic energy was compared at close to free surface cases, results showed faster spreading and quicker mixing of the jet due to the imposed swirl on

the jet. Maximum change in turbulent kinetic energy was seen at s=0.265, smallest for s=0.50, and intermediate for s=0.522.

Minimal studies have been completed, that include a swirl jet into a crossflow. Kalfas et al. [8] studied the flow domain and characteristics of a swirled jet in crossflow at incompressible conditions through computational analysis on FLUENT. More specifically, RANS with Shear Stress Transport (SST) was used with the two equation k-ω model. Their velocity ratios range from 0.75 to 1.3 with swirl numbers varied from 0.0 to 0.4. Results showed that by imposing a swirl on the jet, it would eliminate the formation of symmetric kidney vortex core. For high swirl numbers, s= 0.4, results showed the destruction of the CVP and the dominant kidney shape vortex is transformed into a "comma" shaped vortex. Further analysis showed that the overall jet penetration is reduced with increasing swirl and velocity ratio.

Kalfas et al.'s [9] experiments consisted of experimental and computational analysis of swirl flows into a crossflow at constant blowing ratio. Experimental analysis took place in a closed loop wind tunnel and measurements were obtained with a five-hole probe with cobra head. Flow visualization was achieved through the injection of dyes and oils. Computational analyses were performed using RANS. Three velocity ratios of 0.75, 1.00, and 1.25 were used with results obtained up to a distance normalized by the orifice diameter of 1.00 with swirl numbers ranging from 0.25 to 1. Their results demonstrated that the CVP will increase in asymmetry as the swirl number increases until the point that the CVP is completely destroyed. The swirl number of 0.5 showed the complete destruction of the right kidney vortex with velocity ratios of 1.25 and less. It

was shown that the jet trajectory bends in the direction of the swirl to keep its angular momentum.

1.1.5 Jet Trajectory

A general equation for the trajectory of jet is in the form of:

$$y^* = Ax^{*m} \quad [2]$$

where y* and x* are scaled vertical and axial distances with d, rd, or r^2d (r being velocity ratio and d being jet diameter). Pratte and Baines [10] found A to be 2.05 and m to be 0.28 for velocity ratios of r=5 to r=25 with an extruded jet. When log-log plots are used with the previous formulation, A becomes the y–intercept and m becomes the slope of a linear line. The slope of the line, m, would be a direct indication of the jets entrainment with the crossflow.

Smith and Mungal [2] focused on the mixing structure of the JICF whose velocity ratios, r, ranged from 5 to 25 emerging from a flushed surface. Results illustrate that structure formation of the CVP corresponds to the enhanced mixing in the near field whereas in the far field the CVP itself is not affected as much. It was suggested that using rd scaling was far more advantageous than using d, as the jet trajectories do not collapse completely. The maximum centerline concentration decay when plotted against s/rd where s was the centerline trajectory showed that in the near field it would decay at a rate of $s^{-1.3}$ vs. $s^{-2/3}$ in the far field, where the two regions are separated at $s/r^2d=0.3$.

1.2 Present Work

In the current numerical model, coil inserts of two different lengths of length to pipe diameter of L/D=2 and L/D=11.25 were introduced in the inner wall of a pipe jet. For each coil inset, velocity ratios, r, were 0.5, 1, 2, 5 and results were obtained up to an axial

distance of x/D= 16. Results were compared with the corresponding results for a smooth jet. To my knowledge, this is the first numerical investigation for a jet in crossflow with coil inserts.

CHAPTER 2

METHODOLOGY

Computational fluids dynamics program of StarCCM+, software by CD-Adapco, was used for this study. StarCCM+ uses continuum based modeling along with numerical algorithms to derive a solution. The numerical model was defined using the boundary and initial conditions with a corresponding solid model. A CAD model representative of the investigation at hand was developed using SolidWorks software and imported into StarCCM+.

Two different models were used in the investigations. Model A consisted of a wind tunnel with overall dimensions of inlet cross section of 60" by 60" and a length of 120". The pipe insert was of length 12D and it was placed perpendicular to the flow at about 10D downstream of the wind tunnel inlet to the working area. In order to simulate an elevated jet, the pipe was extended into the crossflow a total of 2.125D. Figure 2 provides the front and top views of model A set-up. As illustrated, there is a plate that is about one third above the ground with round leading edge and a sharp trailing edge with a 3^{o} angle to prevent reverse flow. For further clarification, the front view is considered the entrance of the crossflow and the x-axis is along the axial mean crossflow velocity. The y-axis runs from bottom to top and the z-axis runs from left to right as seen in Figure 2. Figure 3 shows a closer look at the pipe with the coil insert from a skewed front view. An important note is that the origin of the coordinate system is taken at the center of the

pipe outlet. The coil starts at the edge of the inner pipe wall with a direction of clockwise when looked from the top.

Model B, shown in Figure 4, consisted of an extension in height by 6" and the pipe was extended to 20D, however, still only protruded 4.25" from the mid plate. Other parameters are the same as in model A. These modifications were needed to accommodate the second case of coil insert of L/D=2, where fully developed flow was needed before the flow reaches the coil. For the coil with L/D=11.25 it was not necessary to allow the flow to become fully developed since the length of the coil insert was long enough to have the flow developed within the coiled section.

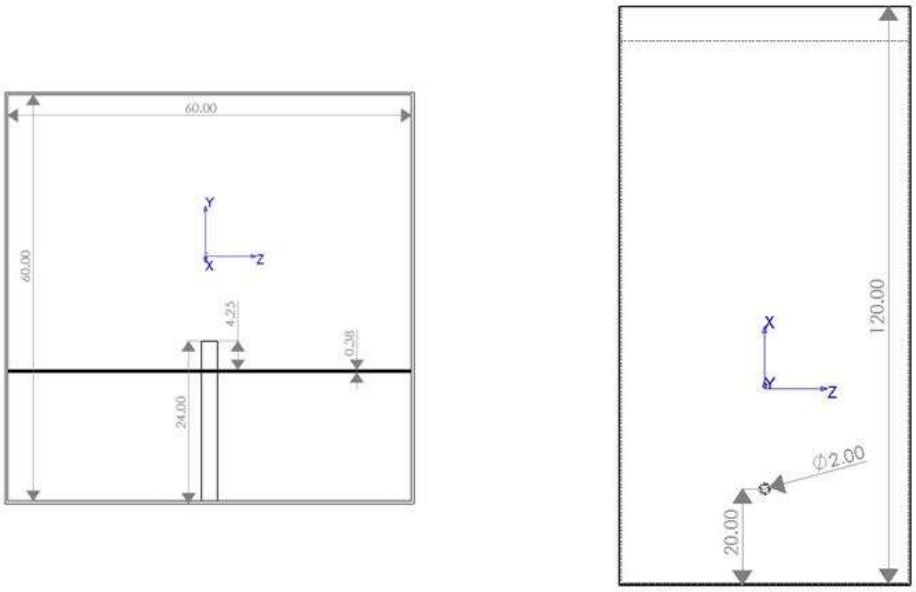

FIGURE 2. Schematic of model A used in CFD, left is front view, right is top view.

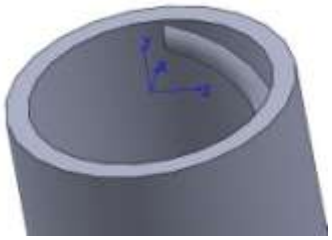

FIGURE 3. Top view of the pipe.

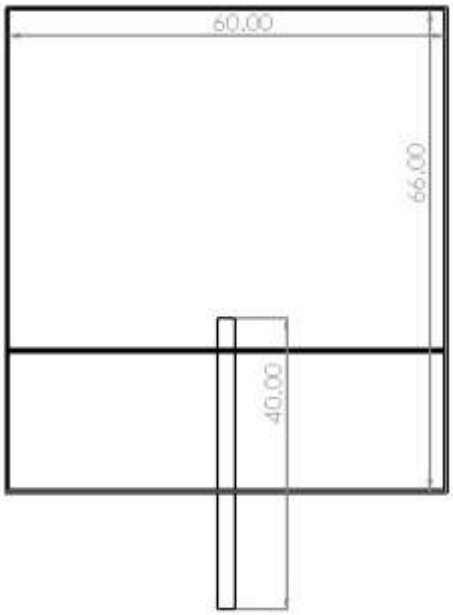

FIGURE 4. Model B modifications.

2.1 Equations and Turbulence Model

StarCCM+ has various physical models for different applications. In the present case, the model is of three-dimension, steady, turbulent, and single phase flow. Air is the working fluid and would be treated as constant density with the inlet temperature at 300K and no heat was added. Given that the current investigations are within the subsonic range, segregated flow with segregated fluid temperature models were used. The K-ω turbulence model was used in all investigations. The K-ω model is based on two main

terms: the k term (the turbulent kinetic energy) and the ω term (the specific dissipation rate) which is the dissipation rate divided by turbulent kinetic energy. The basic K-ω equations, more specifically the SST (Shear Stress Transport) K-ω model are as follows:

$$\frac{d}{dt}\int_V \rho k dV + \int_A \rho k(\mathbf{v}-\mathbf{v}_g)\cdot d\boldsymbol{a} = \int_A (\mu-\sigma_k\mu_t)\nabla k\cdot d\boldsymbol{a} + \int_V (\gamma_{eff}G_k - \boldsymbol{\gamma}'\rho\beta^* f_\beta\,(\omega k-\omega_o k_o) + S_k)dV \quad [3]$$

$$\frac{d}{dt}\int_V \rho\omega dV + \int_A \rho\omega(\mathbf{v}-\mathbf{v}_g)\cdot d\boldsymbol{a} = \int_A (\mu-\sigma_\omega\mu_t)\nabla\omega\cdot d\boldsymbol{a} + \int_V (G_\omega - \rho\beta f_\beta\,(\omega^2-\omega_o^2) + D_w + S_\omega)dV \quad [4]$$

$$G_k = \mu_t f_c S^2 - \frac{2}{3}\rho k\nabla\cdot\mathbf{v} - \frac{2}{3}\mu_t(\nabla\cdot\mathbf{v})^2 \quad [5]$$

$$S = |\boldsymbol{S}| = \sqrt{2\boldsymbol{S}:\boldsymbol{S}^T} = \sqrt{2\boldsymbol{S}:\boldsymbol{S}} \quad [6]$$

$$\boldsymbol{S} = \frac{1}{2}(\nabla\mathbf{v} + \nabla\mathbf{v}^{\mathrm{T}}) \quad [7]$$

$$G_\omega = \rho\gamma\left[\left(S^2 - \frac{2}{3}(\nabla\cdot\mathbf{v})^2\right) - \frac{2}{3}\omega\nabla\cdot\mathbf{v}\right] \quad [8]$$

$$\gamma' = min\left[max\left(\gamma_{eff}0.1\right),1\right] \quad [9]$$

$$D_w = 2(1-F_1)\rho\sigma_{\bar{\omega}2}\frac{1}{\omega}\nabla k\cdot\nabla\omega \quad [10]$$

Here, G_k and G_w are the turbulent production terms, S is the modulus of mean strain rate tensor, and S_k and S_ω are the user-specified source terms. Since the k-ω model is a blend from the k-ω and k-ε model, the introduction of Dw is needed as it is the cross-diffusion term which blends the models together. γ_{eff} is the effective intermittency that is

provided by the Gamma Retheta Transition model on which is unity when model is not activated. F_1 is the blending function which activates Wilcox model near the wall and k-ε model in the free stream. Lastly, β, β*, σ_k, and σ_w are the models coefficients.

Navier-Stokes equations for continuity and momentum:

$$\frac{\partial}{\partial t}\int_V \rho\chi dV + \oint_A \rho(\mathbf{v}-\mathbf{v}_g)\cdot d\boldsymbol{a} = \int_V S_u dV \quad [11]$$

$$\frac{\partial}{\partial t}\int_V \rho\chi\boldsymbol{v} dV + \oint_A \rho\mathbf{v}\otimes(\mathbf{v}-\mathbf{v}_g)\cdot d\boldsymbol{a} = -\oint_A p\boldsymbol{I}\cdot d\boldsymbol{a} + \int_A \boldsymbol{T}\cdot d\boldsymbol{a} + \int_V (\boldsymbol{f_r}+\boldsymbol{f}_g+\boldsymbol{f}_p+\boldsymbol{f}_u+\boldsymbol{f}_\omega+\boldsymbol{f}_L)dV \quad [12]$$

The terms on the left-hand side of [11] are the transient term and the convective flux whereas in the right-hand side are the pressure gradient terms, the viscous flux and the body force terms respectively (**T** is the viscous stress tensor and ***f*** terms are the body forces).

Air for the jet and the crossflow were at standard temperature and pressure along with constant density properties. Models in StarCCM+ used were: 3D –flow, steady flow, turbulent flow, K-ω with SST, segregated flow.

Crossflow mean velocity was constant at 10 ft/s and jet inlet velocity was varied to allow changes in r, allowing for a constant jet diameter of 2 inches. A brief illustration of the mesh is shown in Figure 5 where a volumetric box control named Block 1 is highlighted. The purpose of Block 1 was to further define a volume with refined mesh where the initial details of the flow could be captured. The volumetric box created was altered for different r cases, to accommodate the different spreading and jet entrainment

due to the changes in the velocity ratio. Table 1 shows the run conditions for the twelve different cases.

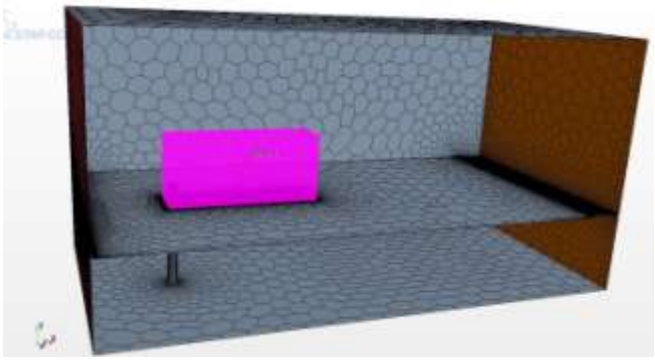

FIGURE 5. Mesh of model with volume Block 1 highlighted.

TABLE 1. Run Conditions for Four Different Velocity Ratios

L/D	r velocity (j) at jet inlet
0	0.5
	1.0
	2.0
	5.0
2	0.5
	1.0
	2.0
	5.0
11.25	0.5
	1.0
	2.0
	5.0

2.2 Grid Dependency

Grid dependency test was done on the models with r=2 with no coil insert and r=5 with L/D=11.25. The specified mesh sizes of the volumetric box used were of 0.14 inch and 0.13 inch. Maximum turbulent kinetic energy and maximum velocity were both monitored; results are shown in Table 2. Assuming less than 5% difference is acceptable,

for all cases studies, increasing the grid size from 0.13 inch to 0.14 inch, results in maximum difference of less than 0.5% in mean velocity and less than 2.2% in TKE. Thus for all cases 0.13 inch grid size was used while for the cases with r=5, 0.14 inch grid size is used.

TABLE 2. Grid Dependency Test Results

		Mesh 0.13 in	Mesh 0.14 in	Percent Difference
r = 2	Maximum Velocity	38.32 ft/s	38.19 ft/s	0.35
	Maximum TKE	3.17 ft^2/s^2	3.21 ft^2/s^2	1.38
r = 5	Maximum Velocity	93.94 ft/s	94.35 ft/s	0.42
	Maximum TKE	19.18 ft^2/s^2	18.77 ft^2/s^2	2.15

2.3 Validation

Validation was completed by comparing current CFD analysis to previous work of Dai et al. [11]. Previous work dealt with using various turbulent models to show which one, better matched experimental results, using a planer jet. For better accuracy, all assumptions and velocities were replicated in the current simulation. The different velocity ratios were accordingly adjusted by keeping the crossflow velocity at 13.9 m/s. Results show that the model created reveal close results with the previous work and can be observed in Figure 6 and Figure 7. Figure 6 shows current results follow the same trend as results from Dai et al. [11]. Comparisons of turbulent kinetic energy shows current results follow a closer trend to that of the experimental results in the near jet exit zone but further downstream same over estimation is seen as in previous publish results.

Further validation was carried out by comparing with results of Orrala and Rahai [12] where they used two side by side jets to investigate the effects of momentum interaction on mixing and jet decay. Their jet trajectory result for a single jet in

crossflow with r=3.3 was compared to the current CFD results as shown in Figure 8. To replicate previous cases, model A was modified by removing the elevated jet portion to simulate a jet issuing from a flushed plane. Results for power equation are shown in Figure 8, and comparisons show that current results under estimate results of Orrala and Rahai [12] by 9%.

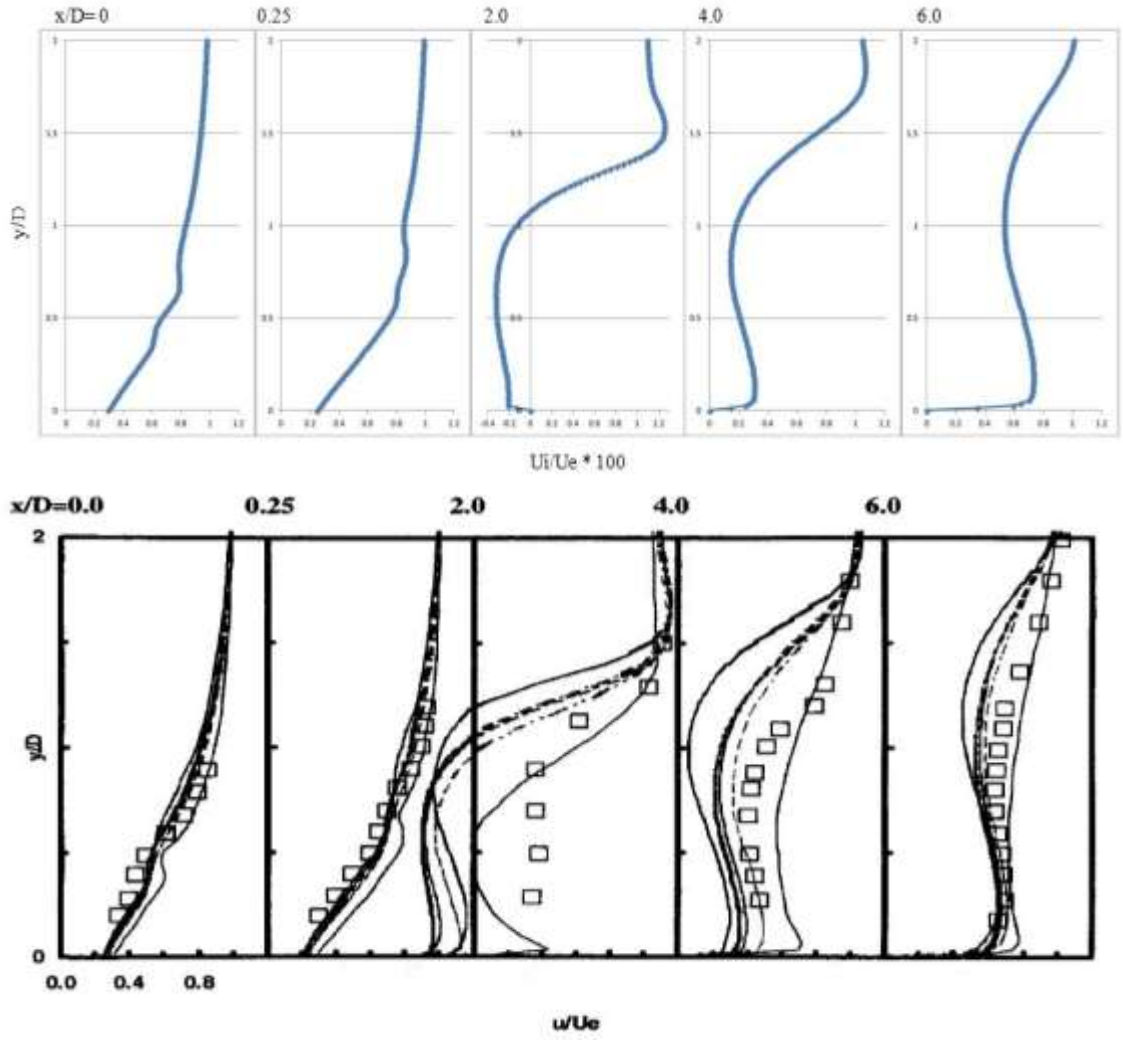

FIGURE 6. Velocity in the axial direction for r=1 taken at centerline (z=0). Top: current CFD results. Bottom: Dai et al.'s [11] results, where square labels are experimental data and lines are CFD results.

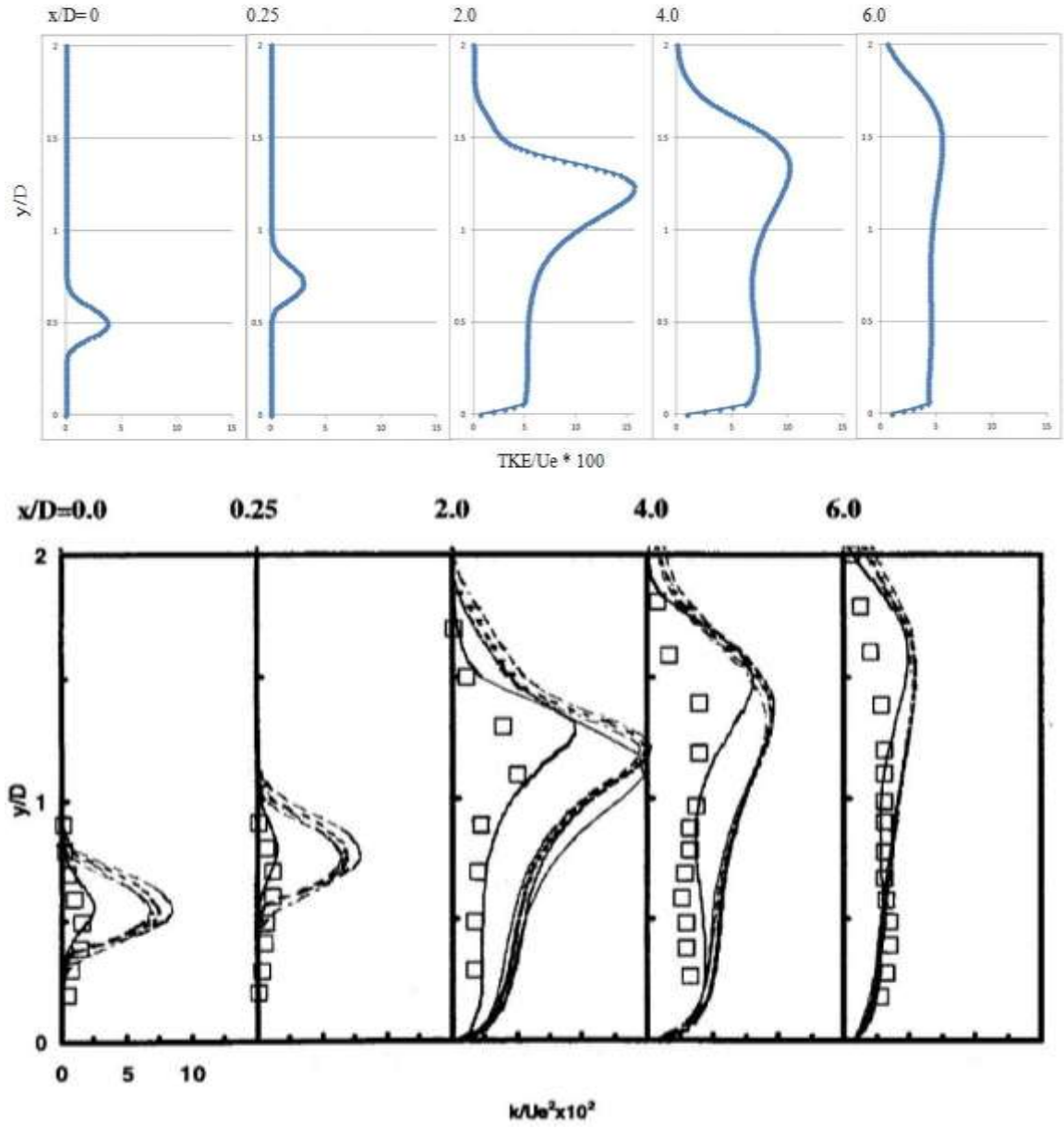

FIGURE 7. TKE for r=1 at centerline (z=0). Top: current CFD results. Bottom: Dai et al.'s [11] results, where square labels are experimental data and lines are CFD results.

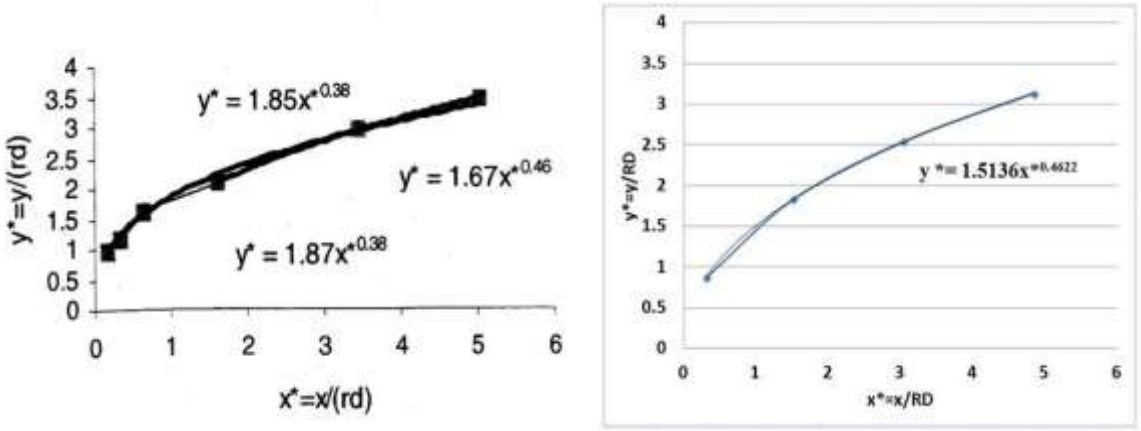

FIGURE 8. Jet trajectory of r=3.3 comparisons of Orrala and Rahai [12] (left) and current CFD results (right) both taken at centerline of CVP, z =0.

CHAPTER 3

RESULTS AND DISCUSSIONS

Results are presented for a pipe jet in crossflow with and without coil inserts at different downstream planes perpendicular to the stream wise flow up to x/D=16. Table 3 shows various cases studied. Here r is the velocity ratio, L/D=0 is for the tube without coil insert and the two coil inserts studied are for L/D=2 and L/D=11.25. The velocity ratio was calculated for the inlet jet velocity (U_j) and the mean exit velocity (U_m) at the jet outlet. Table 3 also includes the corresponding swirl numbers for the jets with coil inserts. As it could be seen in both cases of L/D=2 and L/D=11.25, swirl numbers are weak and coil inserts mostly act as turbulators for mixing enhancement than swirl generator. Swirl numbers for L/D=2 are very weak compared to that of L/D=11.25, due to the shorting in coil length and intern the jet fluid does not develop a stronger swirl.

3.1 Pipe Outlet

Figures 9-11 show contours of the velocity vector for three cases of L/D= 0, 2, and 11.25, for four different velocity ratios of 0.5, 1.0, 2.0, and 5.0. For L/D=0 velocity contours show characteristics of a smooth pipe at high Reynolds number with high velocity dominating most of the mid centers and low velocity near the circumferences. When L/D=2, due to the coil insert, a counter clockwise swirl is imposed on the jet flow. Figure 10 illustrates the velocity vectors at the pipe exit and it can be deducted that the swirl is not centralized.

TABLE 3. Flow Parameters for Different Conditions

L/D	r (Uj)	r (Um)	Re_D	Swirl #
0	0.5	0.46	4539	0
	1.0	0.98	9654	0
	2.0	1.96	19405	0
	5.0	4.95	48971	0
2	0.5	0.49	4803	0.04
	1.0	0.98	9718	0.06
	2.0	1.97	19512	0.08
	5.0	4.98	49220	0.06
11.25	0.5	0.49	4855	0.12
	1.0	0.99	9792	0.18
	2.0	1.99	19671	0.23
	5.0	4.99	49293	0.23

At r=0.5, the location of maximum velocity has shifted toward the upper boundary. When r = 1, in addition to this shift, there is an area of low velocity on the upper boundary and with increasing r, the flow is reduced significantly in this area. When r=5, the flow becomes more uniform within the central section of the tube with reduced velocity near the boundary.

When L/D=11.25, similar results are seen, with the addition of a weak swirl imposed on the flow. These results indicate that for small L/D ratio, the coil acts as an asymmetric turbulator, specially at low velocity ratio, where with increased velocity ratio, the asymmetric behavior is reduced, while at high L/D ratio, the coil mostly acts as a swirl generator, imposing a weak swirl on the flow while still retaining some of the feature of the low L/D coil.

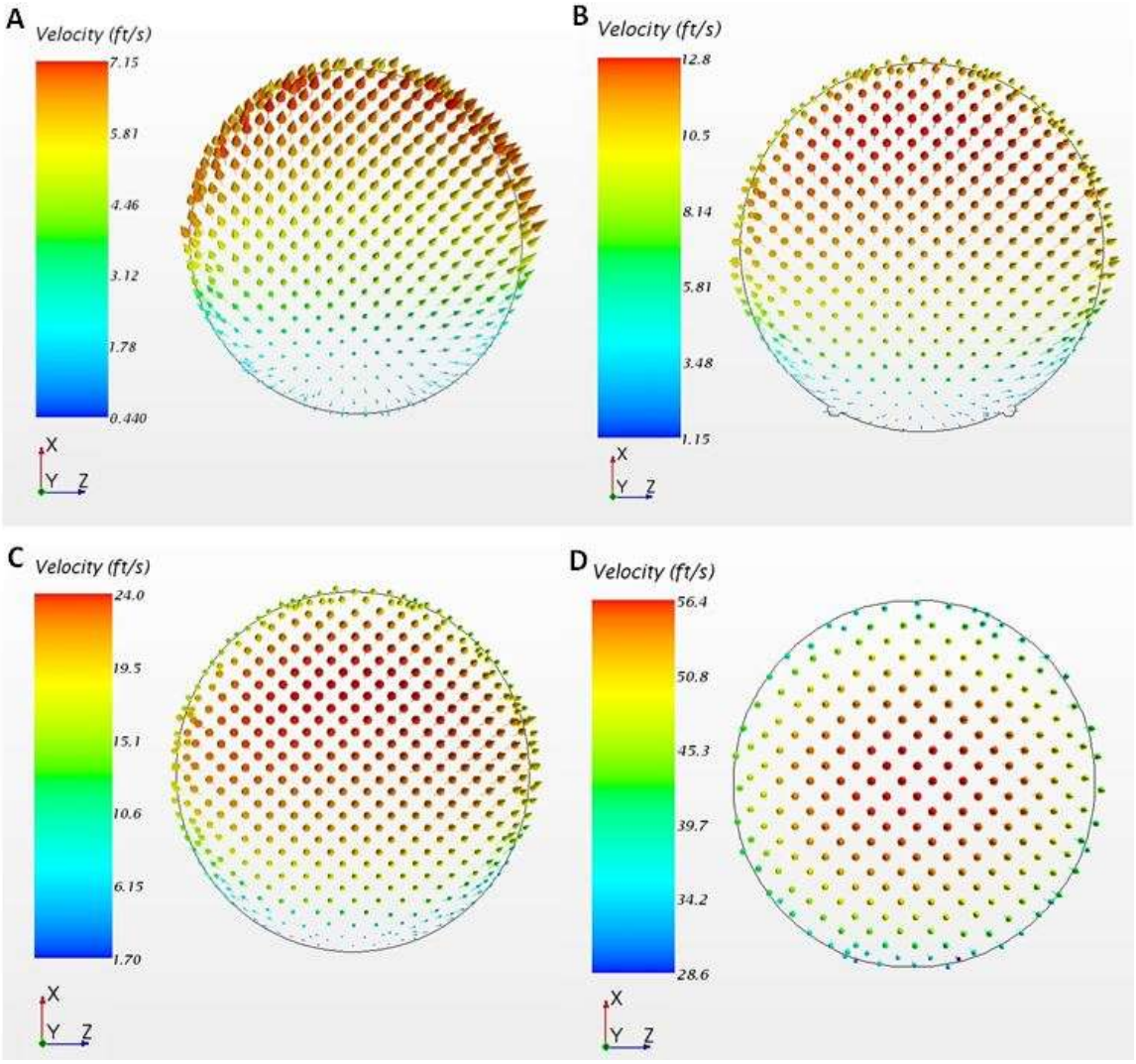

FIGURE 9. Velocity vectors at pipe outlet with non-coil insert of L/D=0. A) r=0.5 B) r=1 C) r=2 D) r=5.

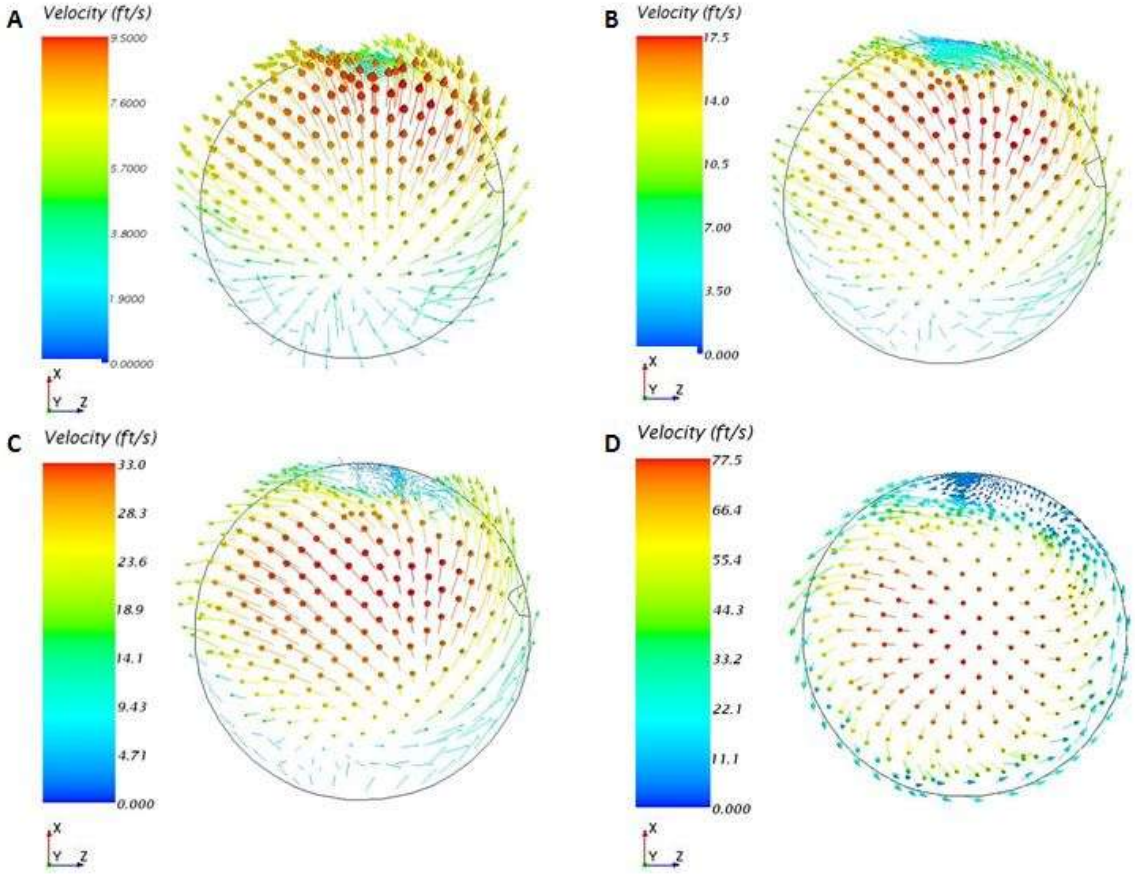

FIGURE 10. Velocity vectors at pipe outlet with coil insert of L/D=2. A) r=0.5 B) r=1 C) r=2 D) r=5.

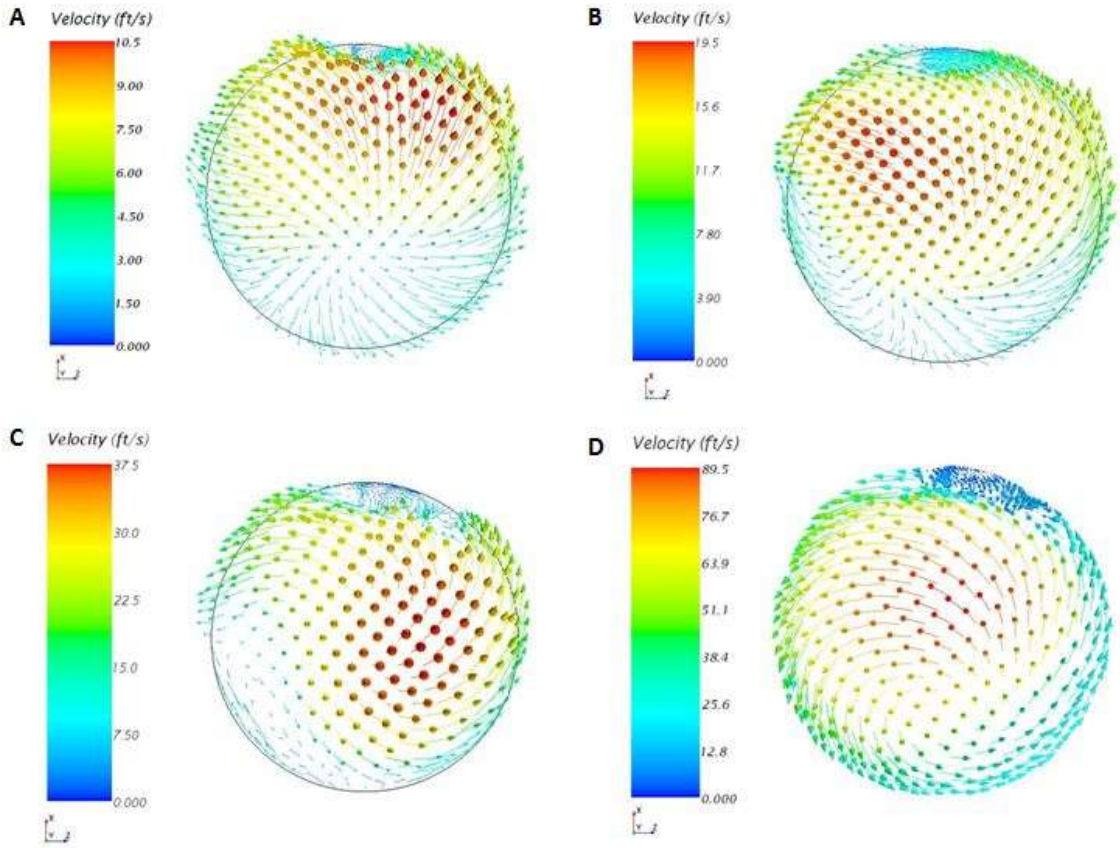

FIGURE 11. Velocity vectors at pipe outlet with coil insert of L/D=11.25. A) r=0.5 B) r=1 C) r=2 D) r=5.

Figure 12 shows an iso-surface created for r=5 and r=0.5 with L/D=0, L/D=2, and L/D=11.25. Initial tilting with both coil inserts are seen to be similar to that of a non coil insert, even though with a coil insert of L/D=11.25 a weak swirl was imposed on the jet. In all cases the formation of what initially seems to be a symmetrical CVP is seen. More profound shear layer vortices dominating in the near field are seen to occur at r=5 with L/D=2. Wake vortices are seen to develop running from the bottom CVP to the mid-plate in all cases. Overall, the dominant features of a jet in crossflow are still evident for a jet with coil insert.

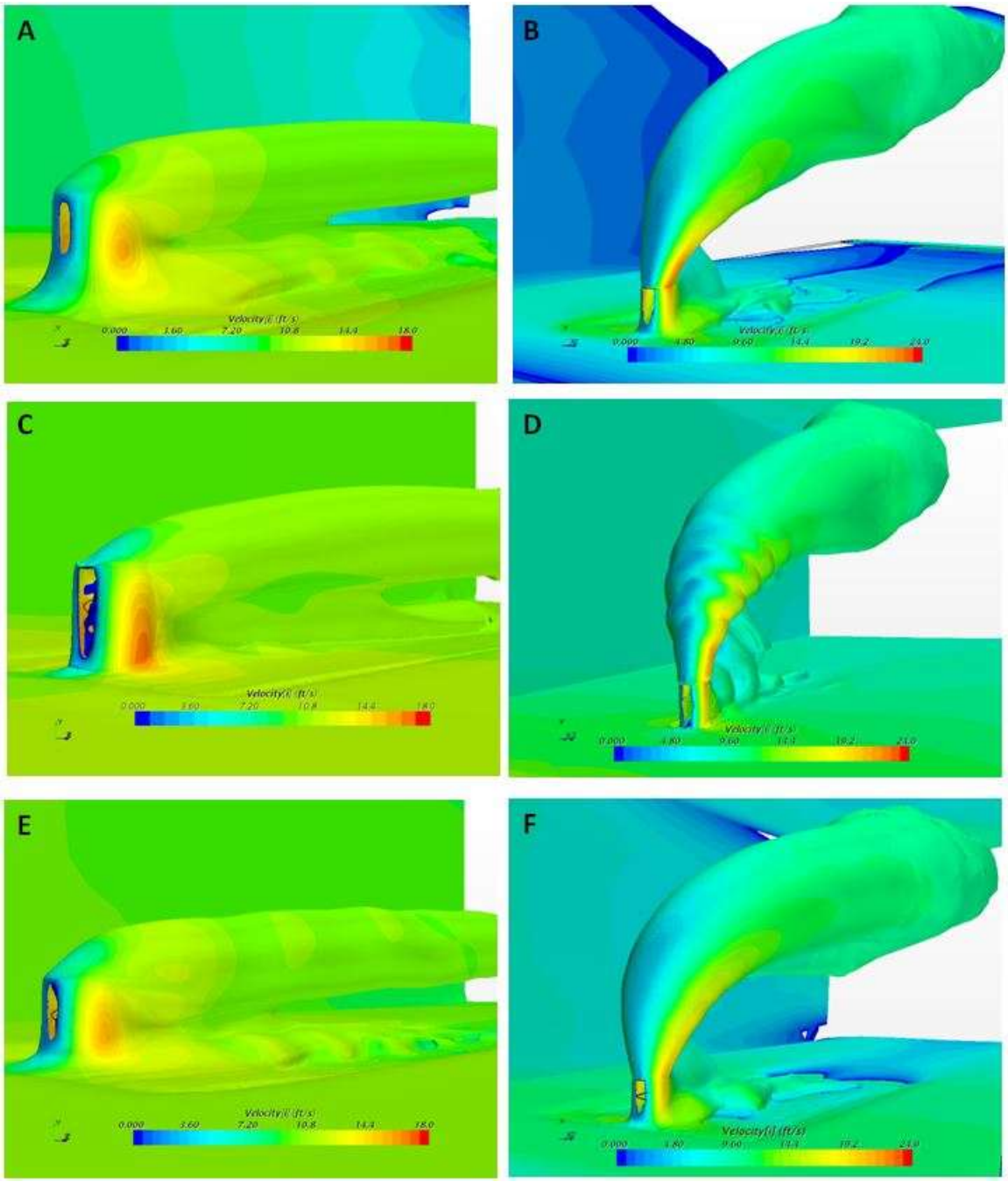

FIGURE 12. Iso-surface from TKE results for axial velocity. A) r=0.5 with L/D=0, B) r=5 with L/D=0, C) r=0.5 with L/D=2, D) r=5 with L/D=2, E) r=0.5 with L/D=11.25, F) r=5 with L/D=11.25.

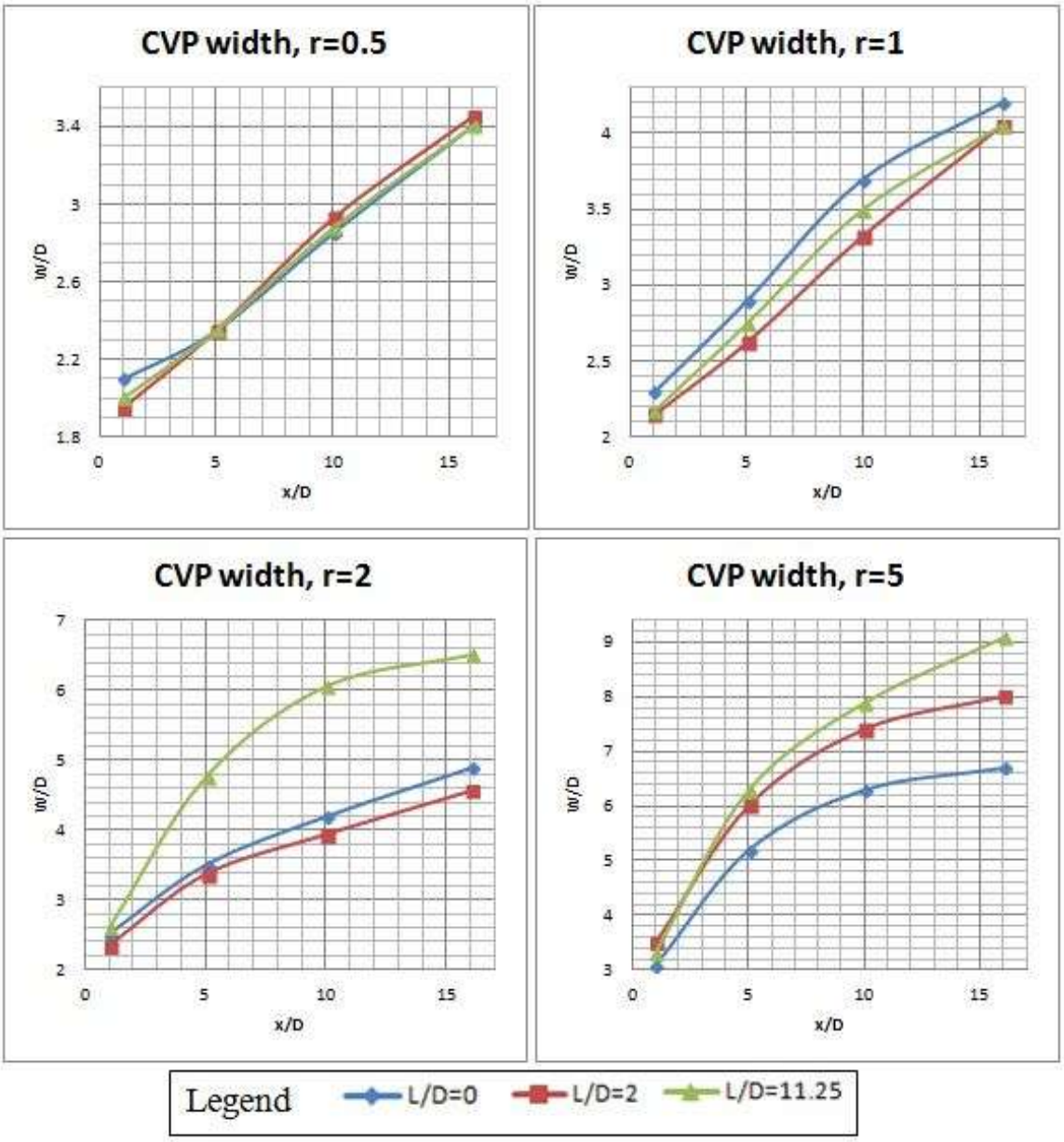

FIGURE 13. CVP widths for all cases.

3.2 CVP Width

Figure 13 shows the width of the CVP formed, with respect to velocity ratio and coil insert, through the effect of the crossflow entrainment on the jet. As shown at r=0.5 there is no significant difference with a coil insert but at r=1 the CVP has a reduction in width

with a coil insert, signifying less mixing between the crossflow and the jet. Increasing velocity to r=2 increased the size the CVP only for L/D=11.25 insert, further increase jet velocity to r=5 allowed greater mixing between the crossflow and jet as the CVP is seen to widen for both coil inserts. Results demonstrate that with a higher velocity ratio the coil insert enhances crossflow entrainment.

3.3 r=0.5

3.3.1 Velocity Vectors

The most noticeable effect of the coil insert on the orifice is the imparity of the counter rotating vortex pair. As seen in Figures 14, 15, and 16, there is still a vortex pair but it is not symmetric. It can be observed the jet penetration in the crossflow is shifted to the left at x/D=1, which is due to the counter rotation imposed on the jet outlet created by the coil insert. Flow being tilted to the left direction is in agreement with Kalfas et al. [9] stating that flow diverts in the direction of the rotation in order to maintain its angular momentum. As the CVP develops downstream, the CVP stays tilted to the left for the coil insert with L/D=2 whereas the CVP is redirected to the right with the coil insert of L/D=11.25. The shift in the CVP for L/D=11.25 can be explained through the Magnus effect where the tangential flow of the outlet swirl is in the same direction as the crossflow (z>0), creating a lower pressure than the opposite side creating suction on the flow.

3.3.2 Turbulent Kinetic Energy

Turbulent kinetic energy does not appear to increase as expected to in the near field. Figure 17 through Figure 19 illustrate the turbulent kinetic energy for the various models at planes of x/D=1 and x/D=5.

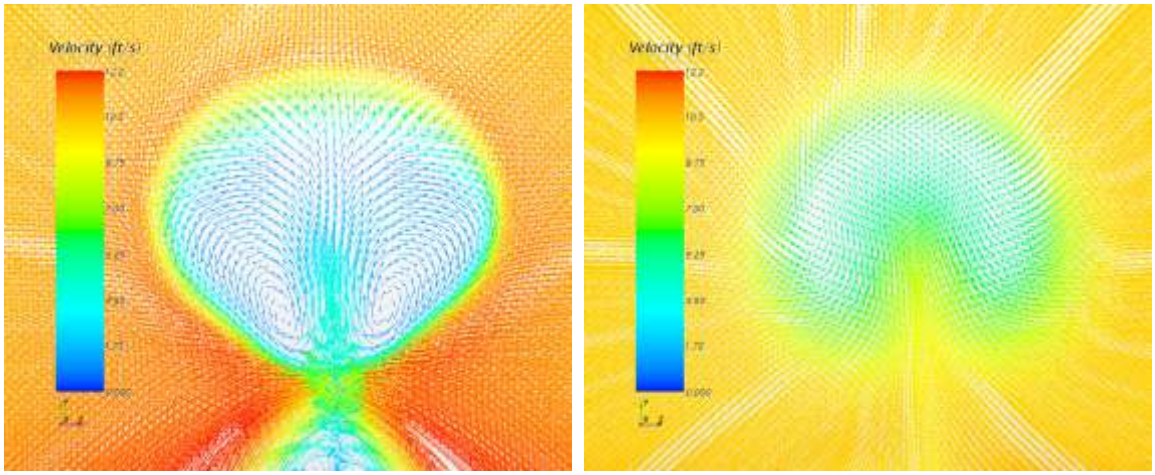

FIGURE 14. Velocity vectors for r=0.5 with L/D=0, left x/D=1, right x/D=5.

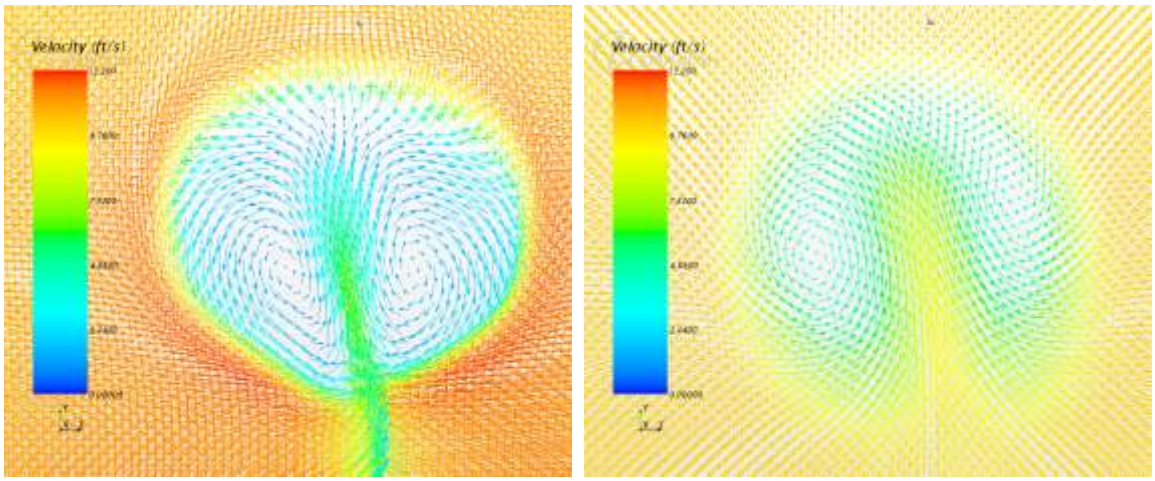

FIGURE 15. Velocity vectors for r=0.5 with L/D=2, left x/D=1, right x/D=5.

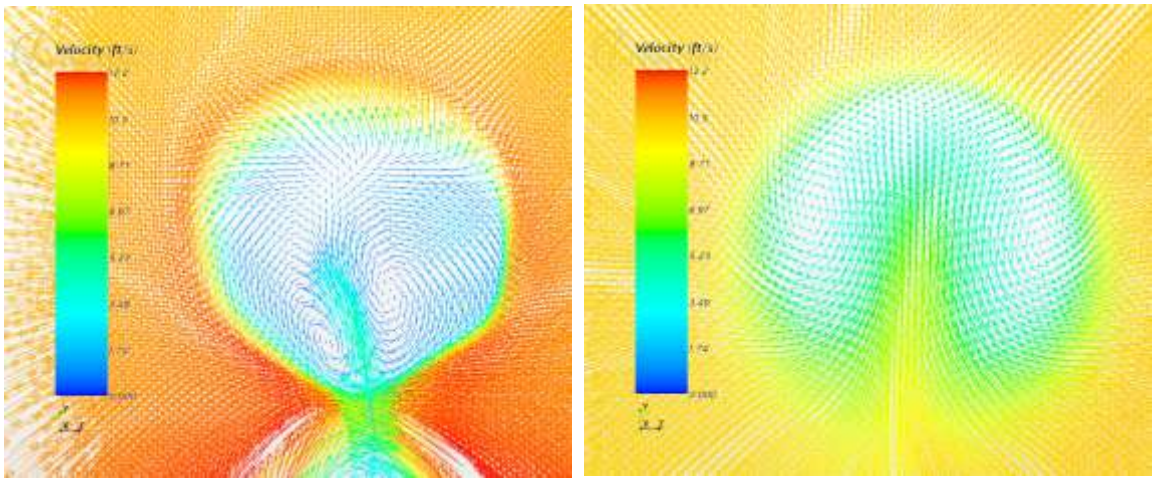

FIGURE 16. Velocity vectors for r=0.5 with L/D=11.25, left x/D=1, right x/D=5.

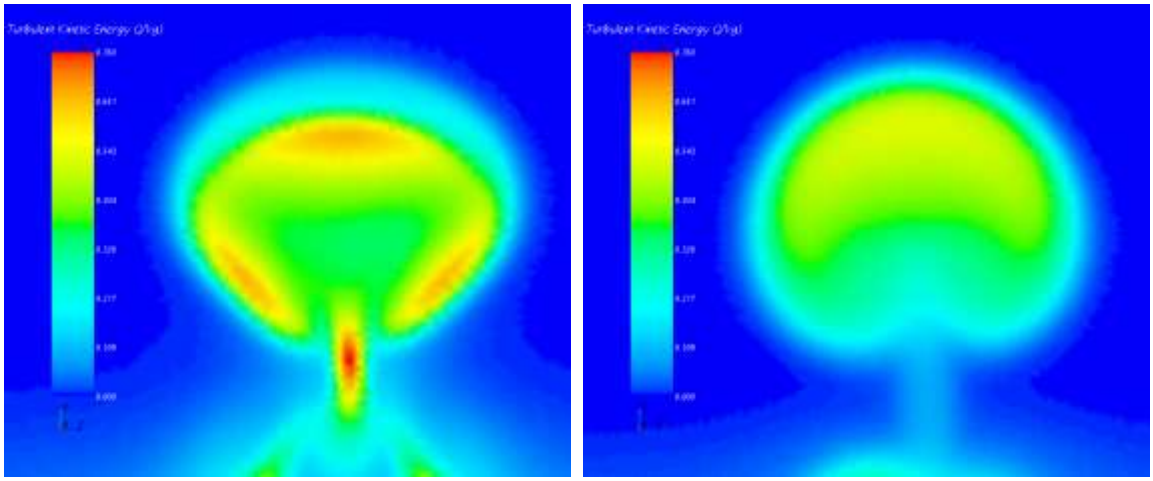

FIGURE 17. TKE for r=0.5 with L/D=0 left x/D=1, right x/D=5.

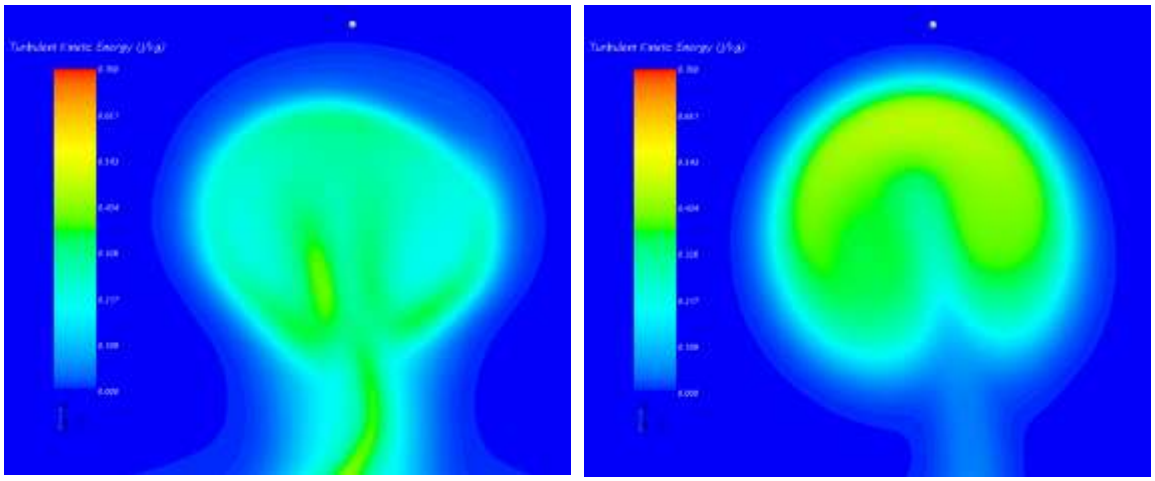

FIGURE 18. TKE for r=0.5 with L/D=2, left x/D=1, right x/D=5.

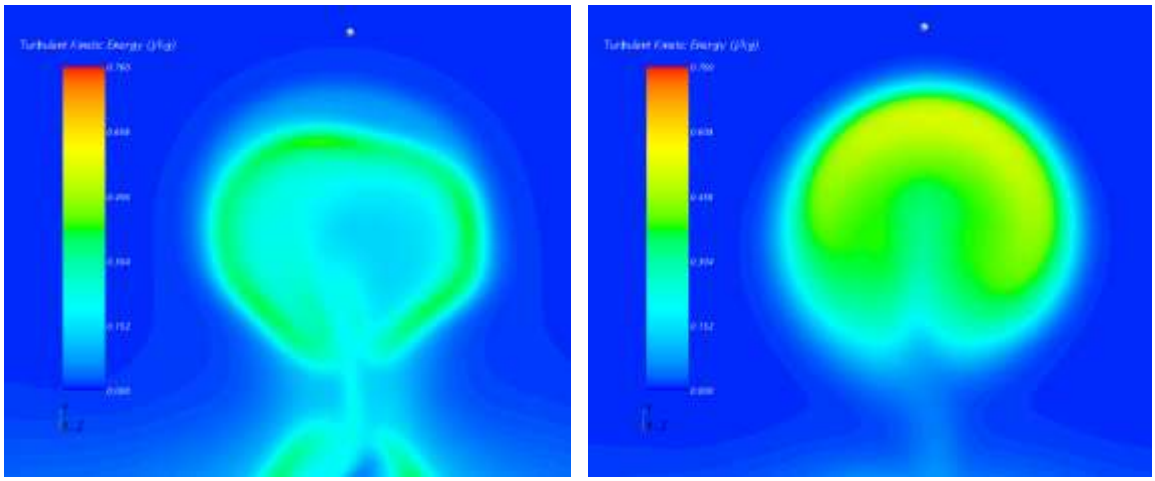

FIGURE 19. TKE for r=0.5 with L/D=11.25, left x/D=1, right x/D=5.

TKE for the smooth pipe is about 40% higher at x/D=1 than with both coil inserts, while at x/D=5, TKE becomes indistinguishable. Further investigation demonstrates that with a coil insert, turbulent kinetic energy holds a higher value downstream at x/D= 10 & 16. TKE was 10% higher with the coil insert of L/D= 2 than with L/D=11.25 at both x/D locations of 10 and 16 concurring with Almoukdad et .al [6] results, where a coil insert of L/D=2 would have a higher TKE downstream as opposed to a coil insert of L/D=11.25. Results in TKE suggest that mixing enhancement is hindered with a coil insert even though higher values are seen further downstream for r=0.5.

3.3.3 Vorticity

The flow field has increased vorticity with coil insert. A greater swirl number correlates to a higher vorticity field as shown in Figure 20-22. With a coil insert of L/D=11.25, a higher vorticity was seen on the right side and could be explained by the counter rotation of flow. By having imposed a counter rotation on the outlet flow, the jet has less resistance to the shear layer where the outlet swirl is in same direction as the crossflow vortex, allowing for a stronger vortex to be created. Vorticity was seen to be 50% higher with L/D=2 and about 100% higher with L/D=11.25 than without the coil insert, but at the far field, at x/D=16, vorticity became in the same for all three cases.

3.3.4 Total Pressure

Total pressure plane views are shown in Figure 23-25 and do not show much differences between all three cases. Total Pressure is defined by the summation of static pressure and dynamic pressure. The lower total pressure within the CVP in all three cases is due to the location of the vortex core.

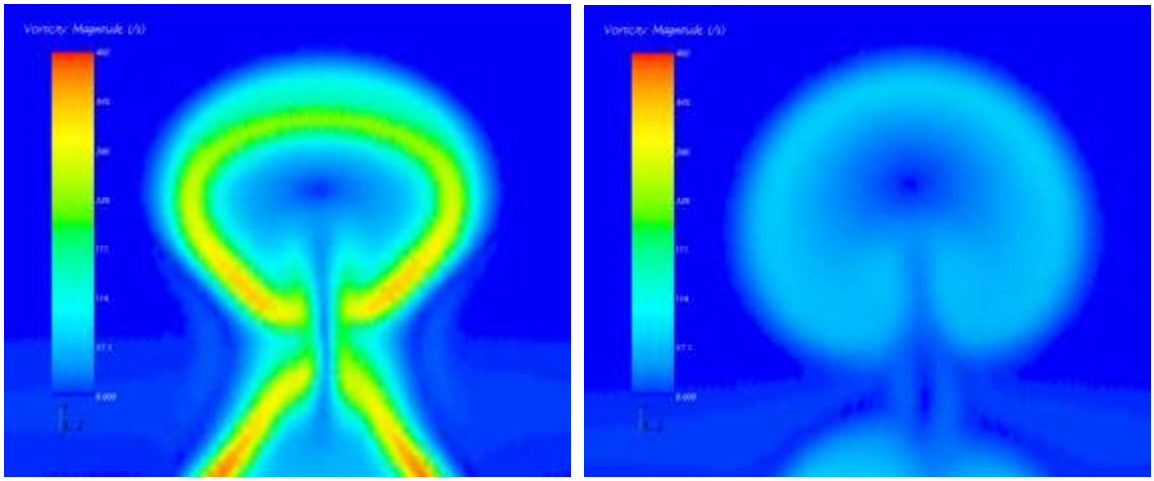

FIGURE 20. Vorticity for r=0.5 with L/D=0, left x/D=1, right x/D=5.

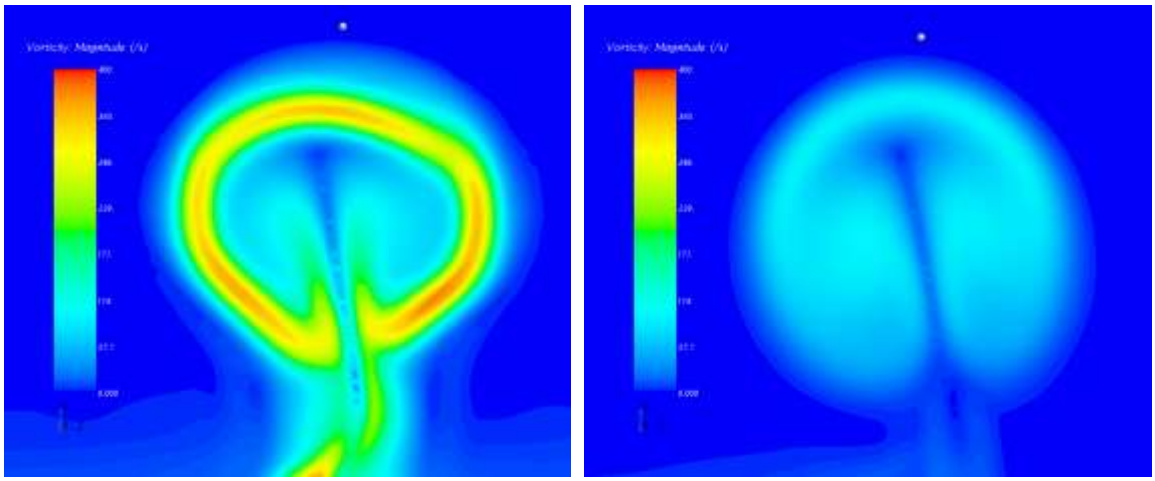

FIGURE 21. Vorticity for r=0.5 with L/D=2, left x/D=1, right x/D=5.

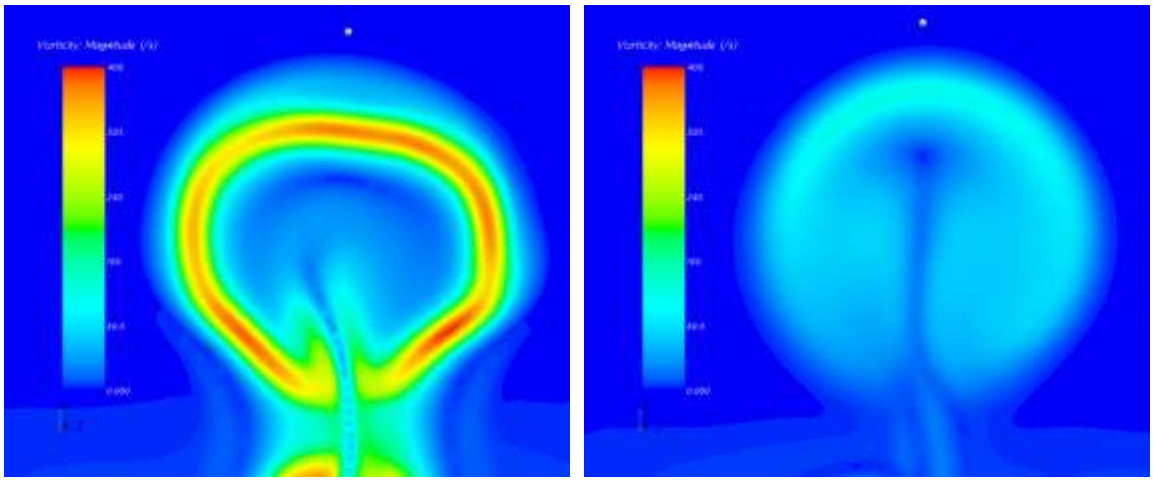

FIGURE 22. Vorticity for r=0.5 with L/D=11.25, left x/D=1, right x/D=5.

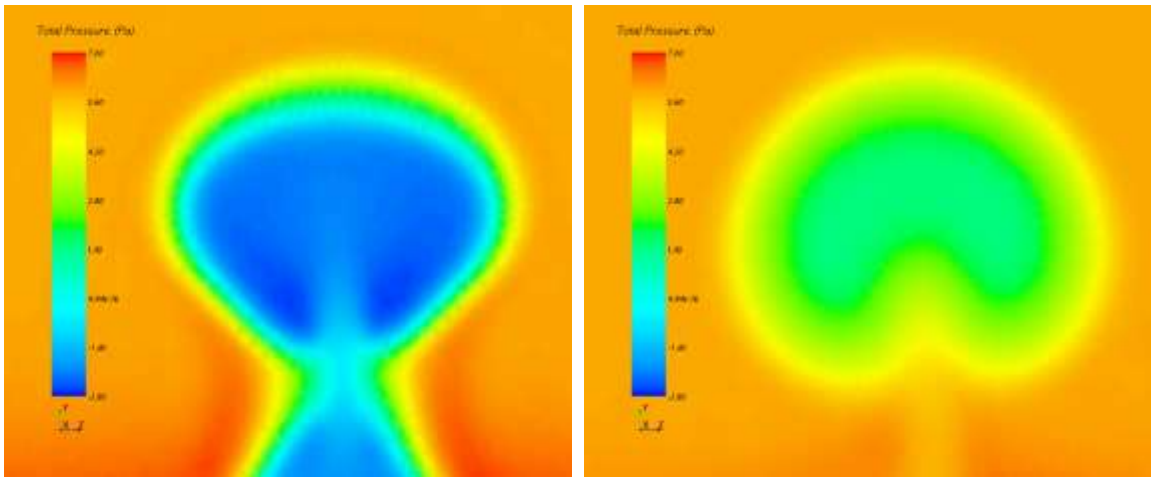

FIGURE 23. Total pressure for r=0.5 with L/D=0 left x/D=1, right x/D=5.

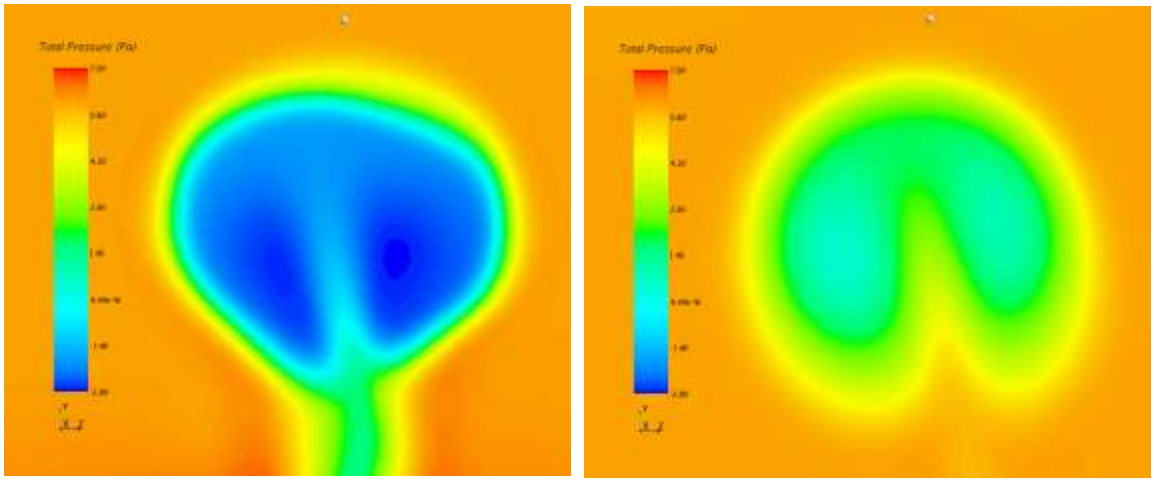

FIGURE 24. Total pressure for r=0.5 with L/D=2, left x/D=1, right x/D=5.

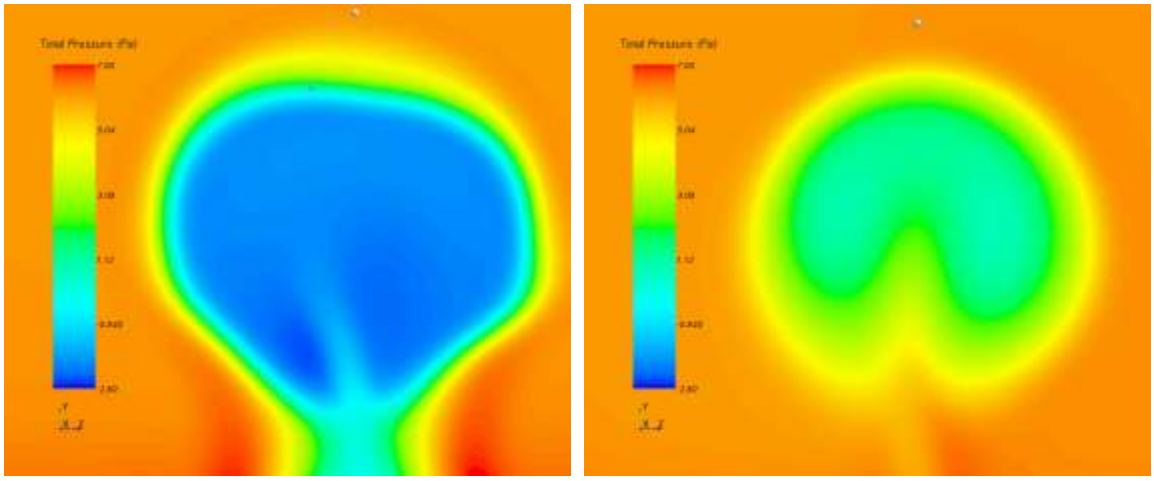

FIGURE 25. Total pressure for r=0.5 with L/D=11.25, left x/D=1, right x/D=5.

3.4 r=1

3.4.1 Velocity Vectors

For velocity ratio of 1, a greater distortion of the symmetrical CVP is visible. For the velocity vectors, Figures 26-28 show that the velocity penetrates further into the rotating vortex pair and it is due to the fact that the coil inserts acts like a nozzle as well allowing the jet to have a higher throw before redirecting in the direction of the crossflow. The coil insert reduces the flow area and creates a nozzle effect on the flow such that with an insert of L/D=11.25 velocity at the jet outlet is higher than that of L/D=2. The increase in coil length creates a swirl number of 0.18 as opposed to 0.06 for the shorter coil. The stronger effect of the swirl is shown by the creation of a more "droopy" left vortex at x/D=5, as shown in Figure 28. The same effect is seen where the asymmetric CVP pair is initially tilted to the left, due to the swirl, as with r=0.5. The velocity fields become similar within the three cases, when examining the flow further downstream from x/D=5 and beyond.

3.4.2 Turbulent Kinetic Energy

As opposed to the velocity ratio of 0.5, TKE with coil inserts have closer values to that of the smooth tube. At x/D=1, TKE for L/D=0 and L/D=11.25 are equal but with L/D=2 TKE is less than both by as much as 25%. As the flow goes past x/D=5, TKE for the jet with coil inserts are nearly the same and about 10% higher than the TKE for the smooth tube. It can be concluded that with coil inserts, near the jet exit, mixing enhancement is reduced due to the decrease in the TKE and reduction in CVP width. Results from further downstream show that both jets with coil inserts maintain a higher TKE at x/D=10 & 16 planes, more specifically at the two further downstream planes, TKE for L/D=11.25 is 10% and for L/D=2 is 20% higher than the smooth tube.

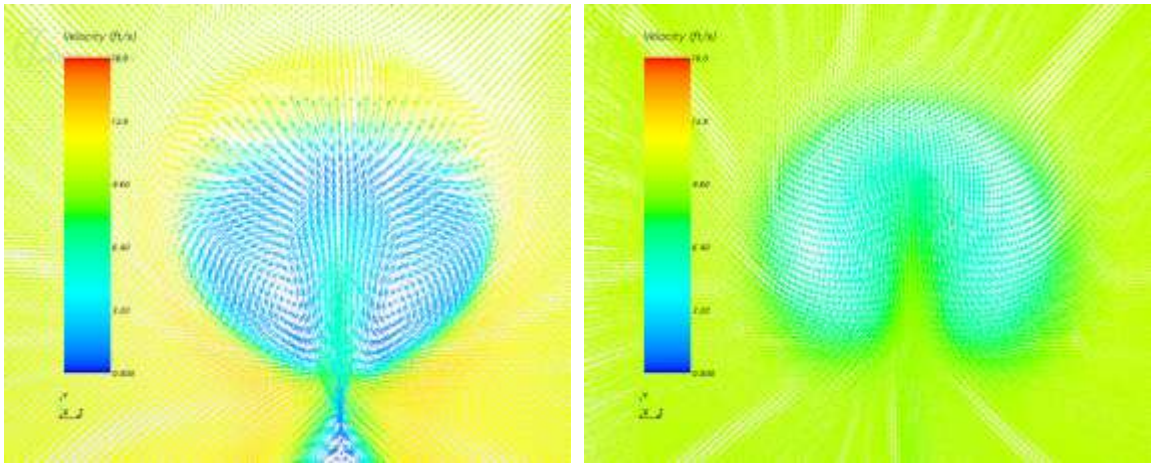

FIGURE 26. Velocity vector for r=1 with L/D=0, left x/D=1, right x/D=5.

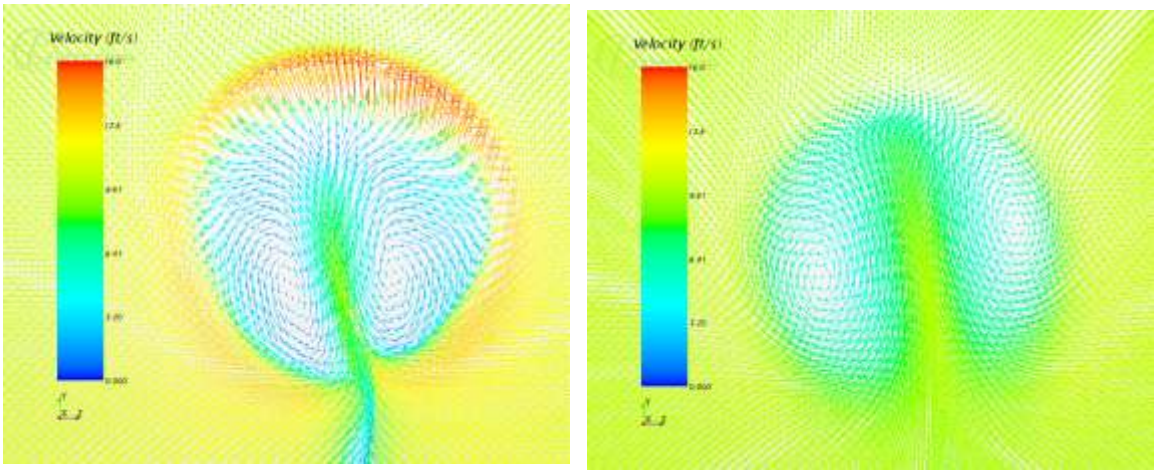

FIGURE 27. Velocity vector for r=1 with L/D=0, left x/D=1, right x/D=5.

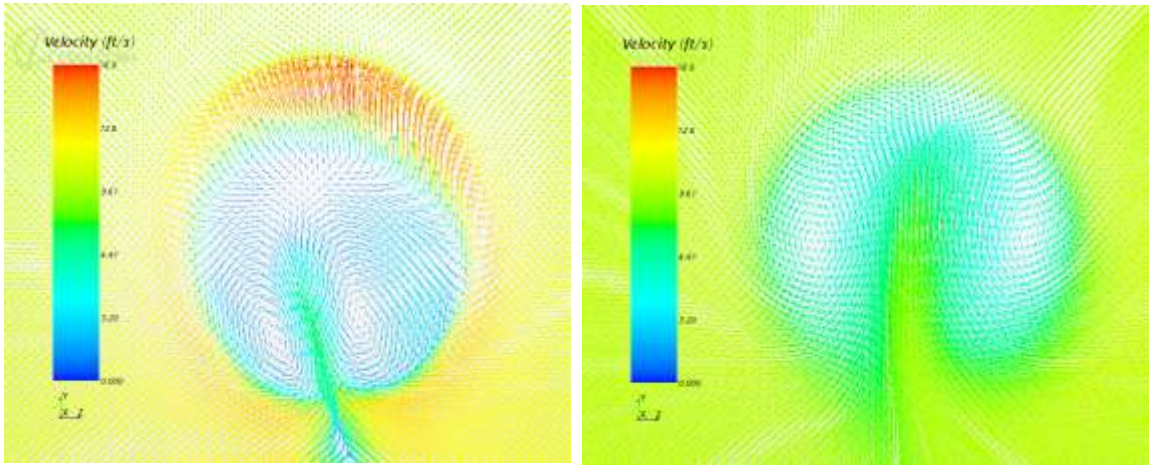

FIGURE 28. Velocity vector for r=1 with L/D=11.25, left x/D=1, right x/D=5.

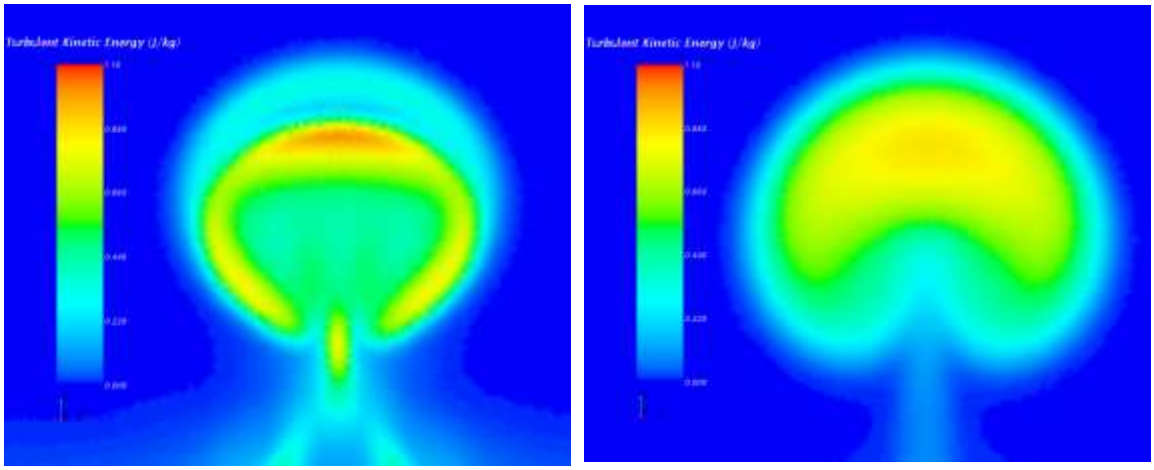

FIGURE 29. TKE for r=1 with L/D=0, left x/D=1, right x/D=5.

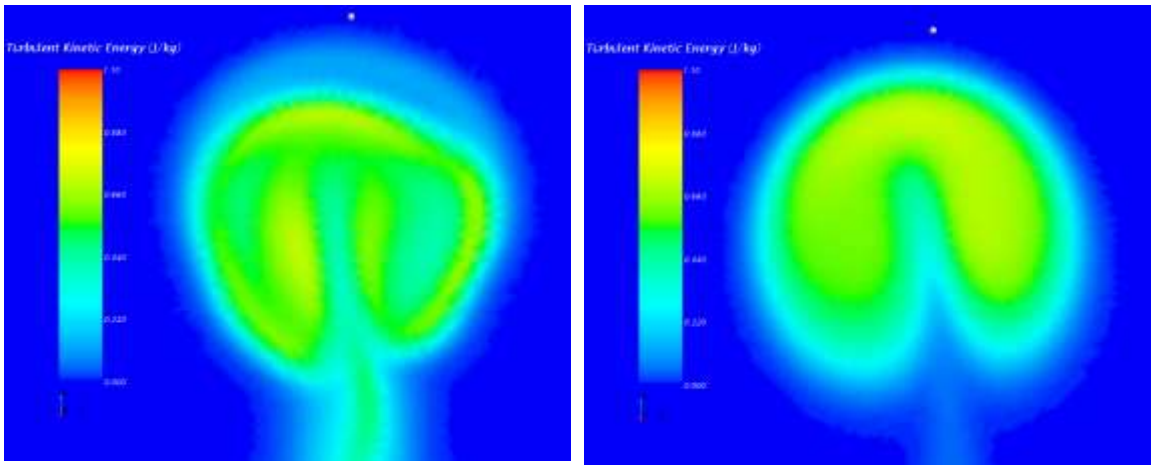

FIGURE 30. TKE for r=1 with L/D=2, left x/D=1, right x/D=5.

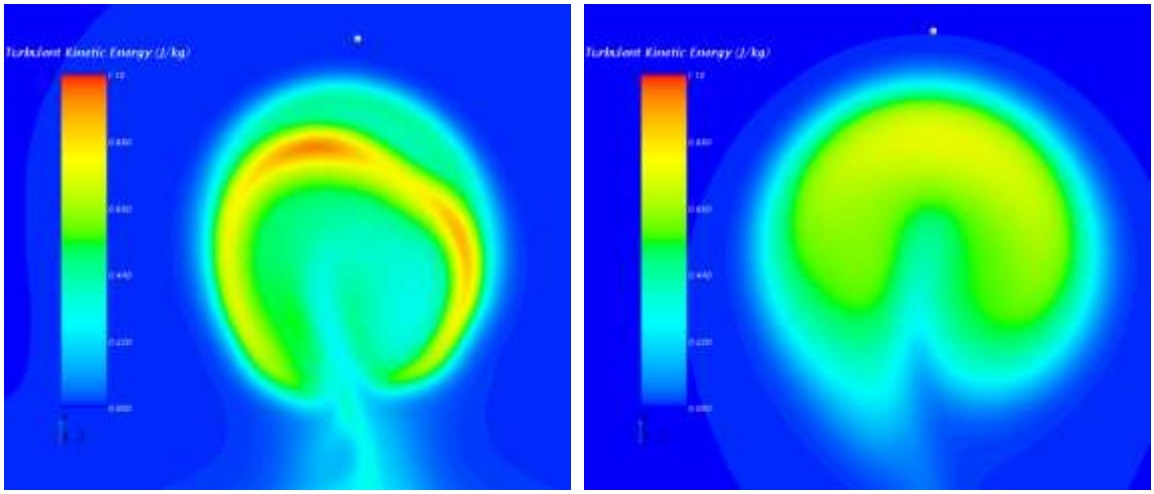

FIGURE 31. TKE for r=1 with L/D=11.25, left x/D=1, right x/D=5.

3.4.3 Vorticity

The highest magnitude in vorticity was with coil insert of L/D=2 at the plane x/D=1 as opposed to r=0.5 where highest vorticity was visible with L/D=11.25. In the far field, at x/D=16, vorticity has reached a constant value with and without coil insert. With coil inserts, at prior axial planes, vorticity is between 30% and 20% higher than the smooth tube for L/D=2 and L/D=11.25 respectfully. Due to the higher vorticity with L/D=2, higher energy potential is retained and released downward resulting in increased TKE.

3.4.4 Total Pressure

Pressure in a vortex should be lowest at the vortex core, as shown in Figures 35-37. When L/D=2, there is a much less value in pressure correlating due to the higher vorticity results. The asymmetry behavior is shown by having a stronger vortex on the right. Pressure differences are only seen at x/D=1 with minimal differences beyond x/D=5.

3.5 r=2

3.5.1 Velocity Vectors

The impedance of the symmetrical CVP is also shown at velocity ratio equal to two, as expected. Figures 38-40 show contours of the velocity vectors for the three cases of the smooth tube, and tubes with coil inserts at r=2. When L/D=2, flow initially tilts in the direction of the swirl but as it develops further it realigns itself with the center line (z=0), attaining more symmetry. It becomes almost a symmetrical CVP from x/D=5 and on. Figure 40 shows the complete distortion of the CVP at s=0.23, with L/D=11.25, and formation of a third vortex.

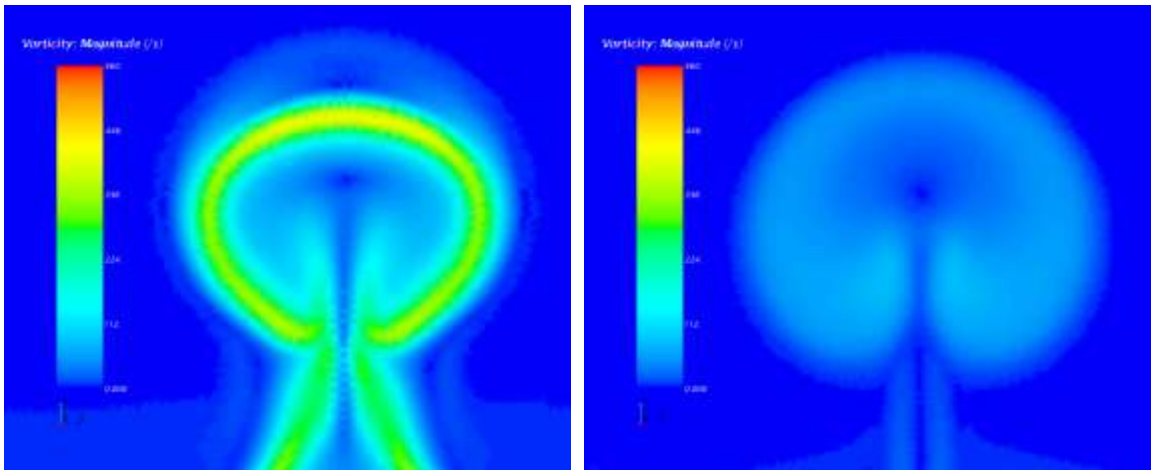

FIGURE 32. Vorticity for r=1 with L/D=0, left x/D=1, right x/D=5.

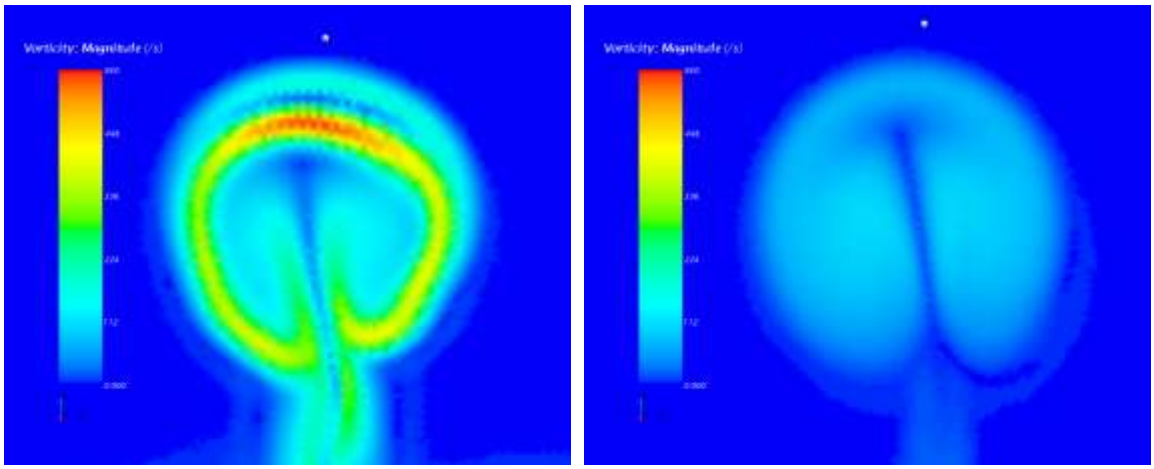

FIGURE 33. Vorticity for r=1 with L/D=2, left x/D=1, right x/D=5.

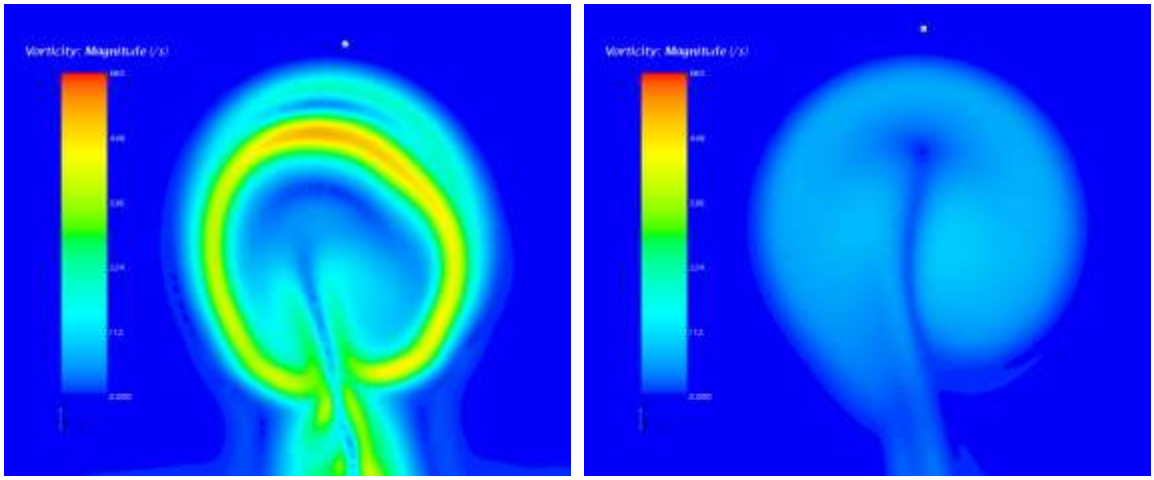

FIGURE 34. Vorticity for r=1 with L/D=11.25, left x/D=1, right x/D=5.

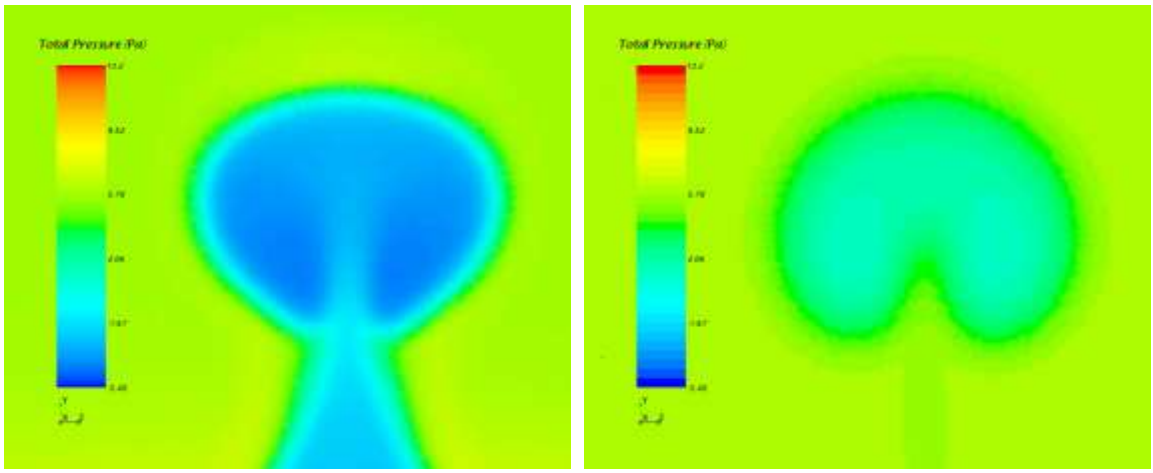

FIGURE 35. Total pressure for r=1 with L/D=0, left x/D=1, right x/D=5.

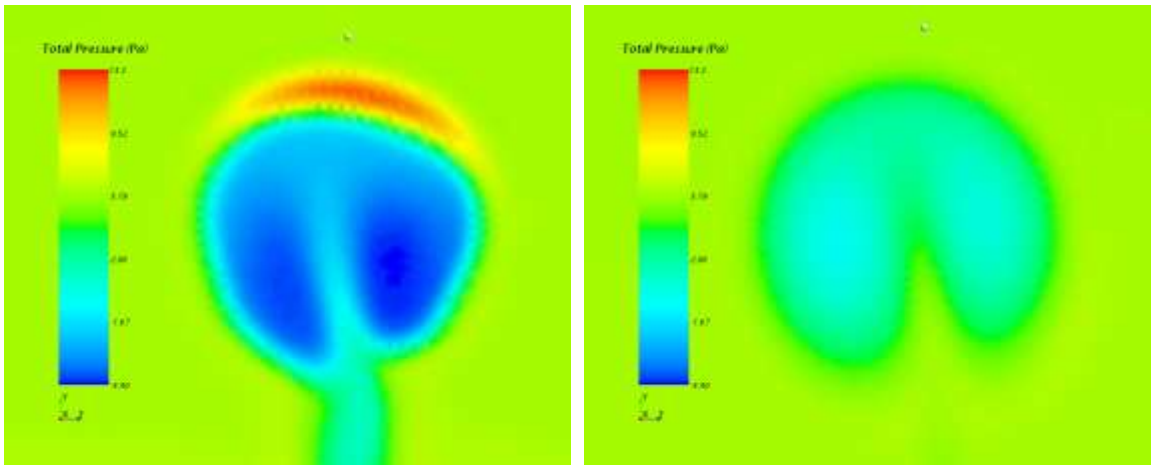

FIGURE 36. Total pressure for r=1 with L/D=2, left x/D=1, right x/D=5.

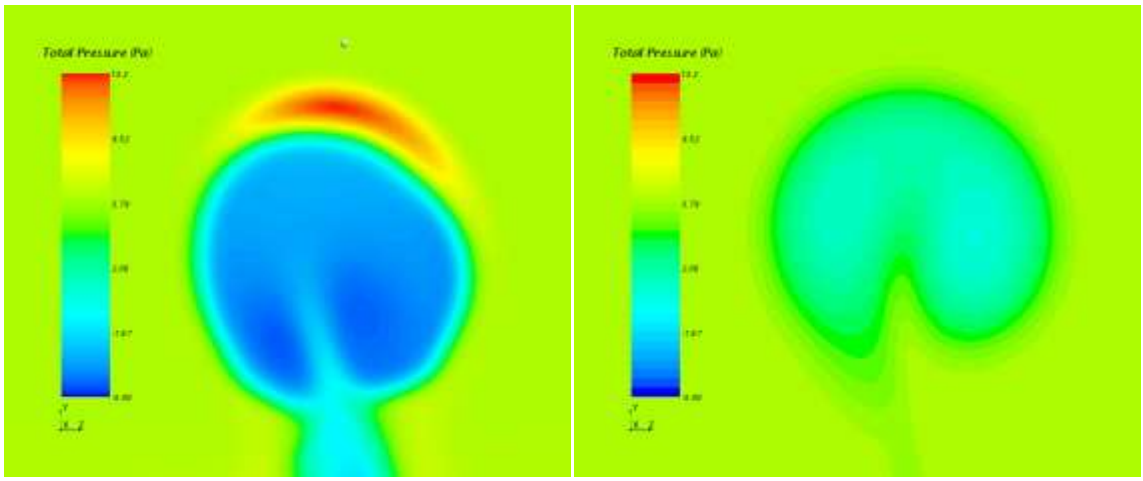

FIGURE 37. Total pressure for r=1 with L/D=11.25, left x/D=1, right x/D=5.

The complete destruction of the kidney shape vortex could be due to velocity at pipe exit, as seen from Figure 10, being concentrated towards the positive z-axis and the formation of the classical CVP is destroyed by having the flow penetrate towards one side of the crossflow. The flow gives an illusion of having a higher throw distance but further analysis explain that the jet narrows and intern could decrease the possibility of the vortex pair formation. Results from Kalfas et al. [8], show that at a high swirl number, the classical CVP is destroyed. Their results showed that at s=0.2 with r=0.8 to r=1.3 an asymmetric CVP is still captured but with s=0.4 the CVP is destroyed for all velocity ratios. The resulting shape, as explained by Kalfas et al. [8], is a comma shape vortex and can be explained by having a strong vortex at bottom with a smaller vortex above it, along the center line. By examining the flow at x/D=1, a vortex at bottom and one at above are seen to start developing but due to the constriction and eccentricity of the outlet flow, a third and higher vortex is formed. Further interaction of the jet and crossflow show the rotation of the flow, as seen in section plane of x/D=5, similar to a CVP but with a third vortex in between. It is to note that at x/D=16, the vortices display a similar shape of an asymmetric CVP and the top initial vortex shrinks to a minimal size.

3.5.2 Turbulent Kinetic Energy

TKE does increase with the coil inset and is much higher than that of smooth tube, when compared with similar results at r=0.5 and r=1. TKE increase by nearly 50% with L/D = 11.25 as compared to 35% increase when L/D = 2. TKE sustains its higher value at x/D=5 with L/D=11.25, while the results for L/D=2 and smooth tube are nearly the same. The increase in TKE allows more crossflow entrainment, explaining the growth of the CVP width.

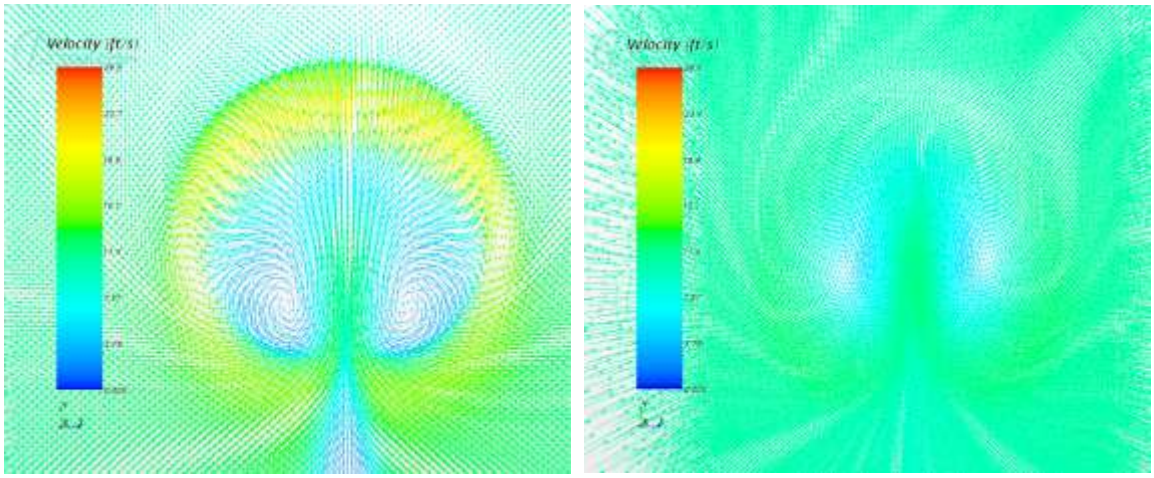

FIGURE 38. Velocity vectors for r=2 with L/D=0, left x/D=1, right x/D=5.

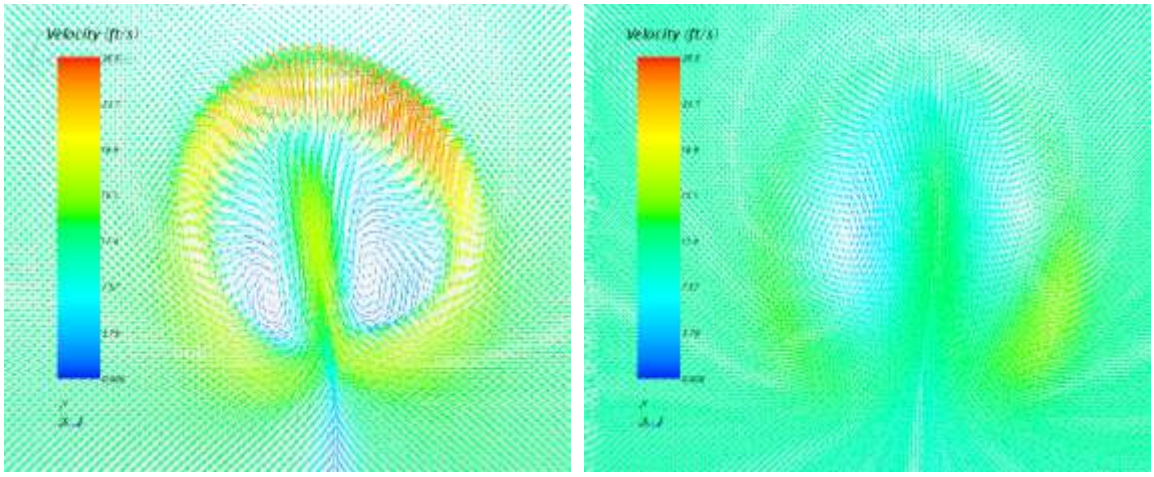

FIGURE 39. Velocity vectors for r=2 with L/D=2, left x/D=1, right x/D=5.

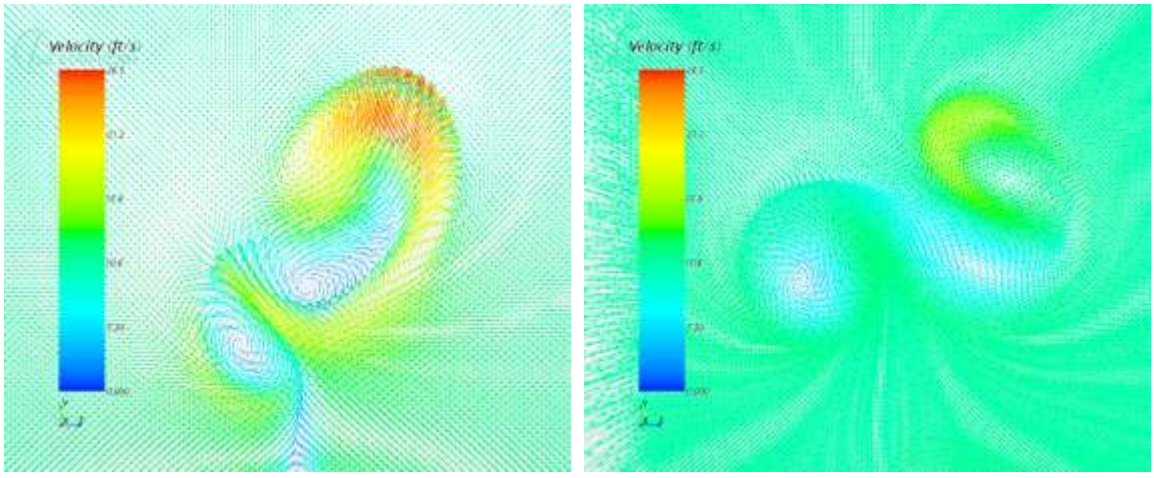

FIGURE 40. Velocity vectors for r=2 with L/D=11.25, left x/D=1, right x/D=5.

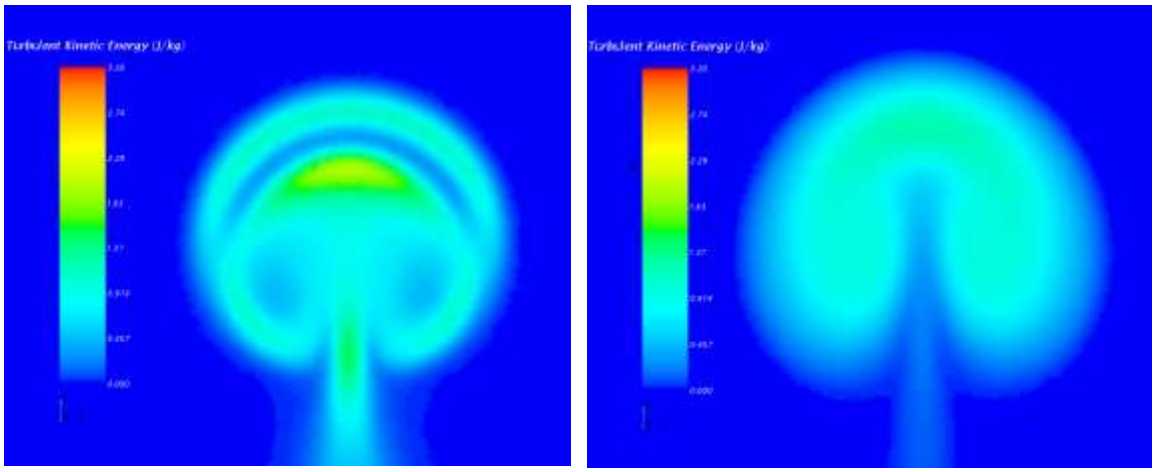

FIGURE 41. TKE for r=2 with L/D=0, left x/D=1, right x/D=5.

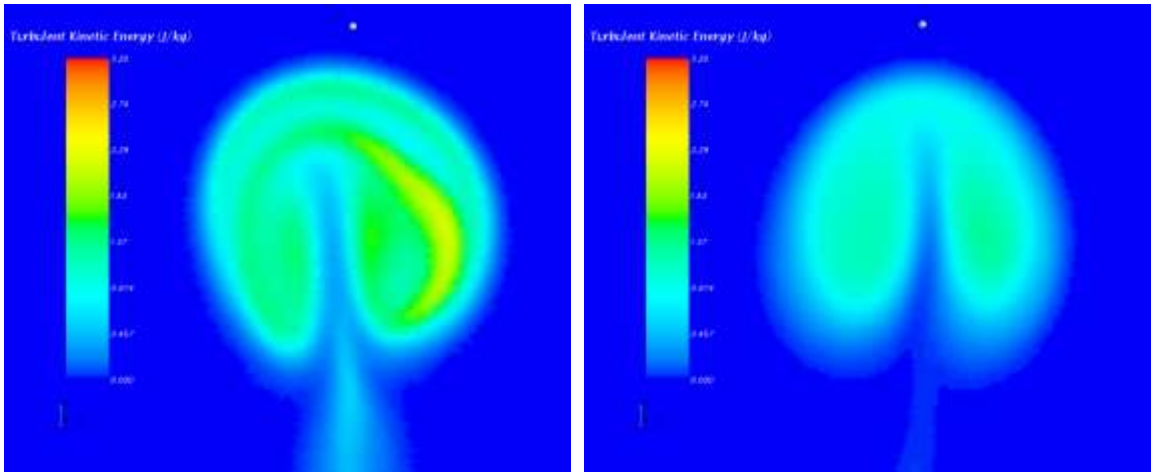

FIGURE 42. TKE for r=2 with L/D=2, left x/D=1, right x/D=5.

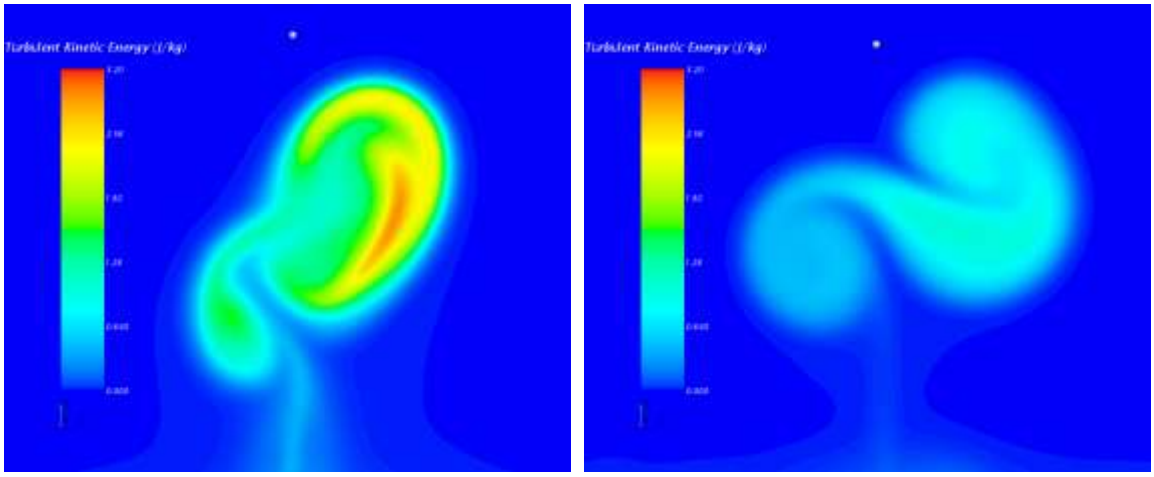

FIGURE 43. TKE for r=2 with L/D=11.25, left x/D=1, right x/D=5.

As it will be shown later on, the increase in TKE corresponds with a decrease in the rate of penetration of the jet into the crossflow. Similar results are seen by Feyedelem and Sarpkaya [7] and Kalfas et al. [8], stating that imposing a swirl will reduce the jet penetration. TKE for L/D=2 becomes highest at x/D=10 & 16, with a value of 15% percent higher than other two cases.

3.5.3Vorticity

Vorticity has the highest value when L/D=2 but at x/D=10, the vorticity value for L/D=11.25 becomes the highest. The energy held in vortices, with L/D=2, is being release in the far field which explains the higher TKE in the far field. Vortex stretching is the main mechanism in which turbulence is increased due to the creation of smaller vortices. Turbulent kinetic energy also increases as the vortices are broken down and release a burst of energy. The high value in vorticity at the top and around the CVP is most likely due to entrainment of crossflow.

3.5.4 Total Pressure

Low pressure is visible at the vortices while high pressure is seen at the points of entrainment, as shown in Figures 47-49. It can be deducted that the strongest vortices occur with L/D=2 as pressure is lowest. High pressure in both flows with coil inserts is the result of the crossflow entrainment. From pressure distribution at x/D=5 for L/D=2, the vortex pair is approaching symmetry but never attain symmetry as the left vortex is remains stronger throughout the flow.

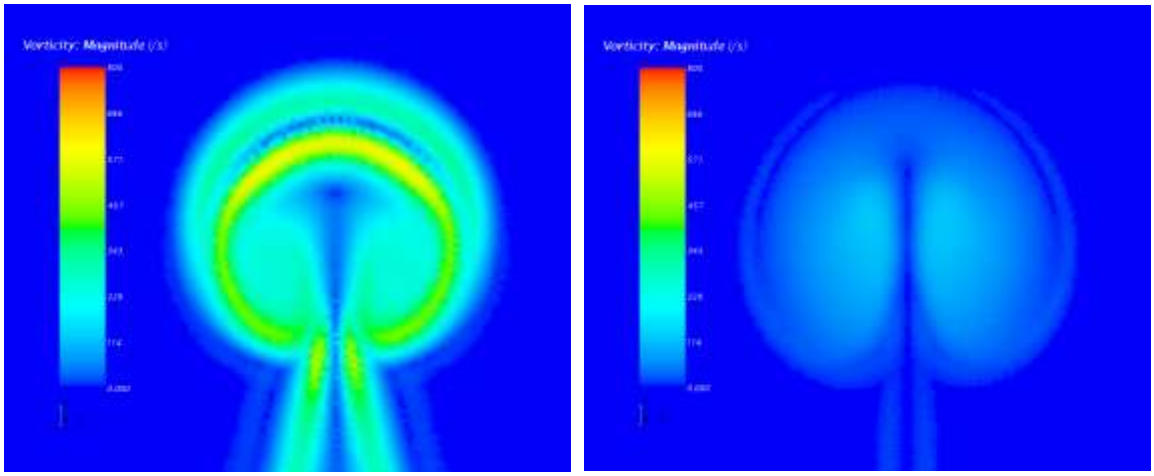

FIGURE 44. Vorticity for r=2 with L/D=0, left x/D=1, right x/D=5.

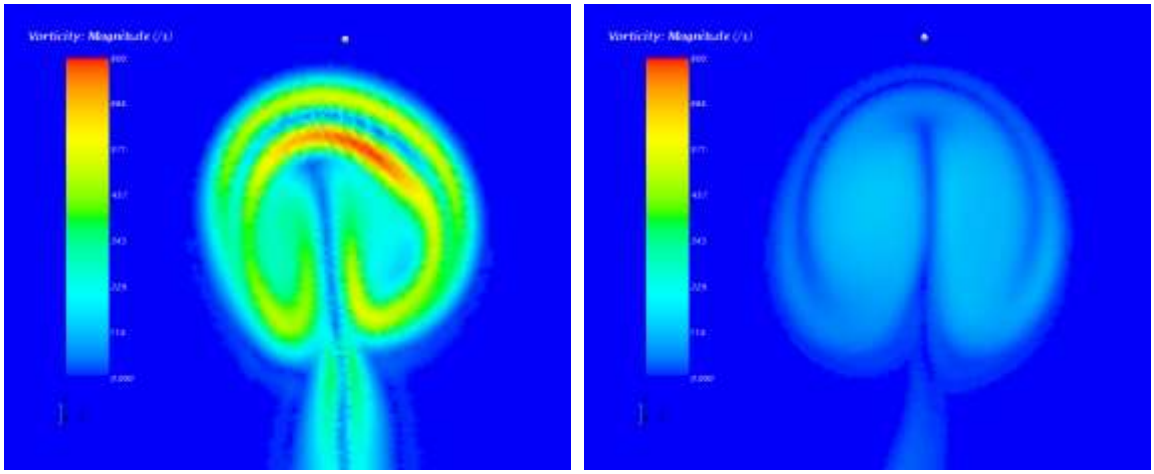

FIGURE 45. Vorticity for r=2 with L/D=2, left x/D=1, right x/D=5.

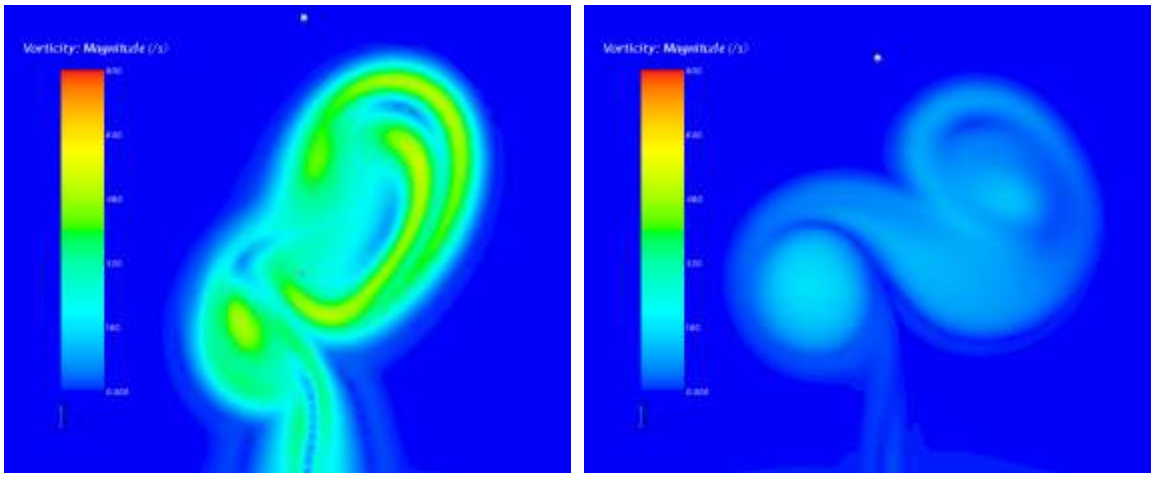

FIGURE 46. Vorticity for r=2 with L/D=11.25, left x/D=1, right x/D=5.

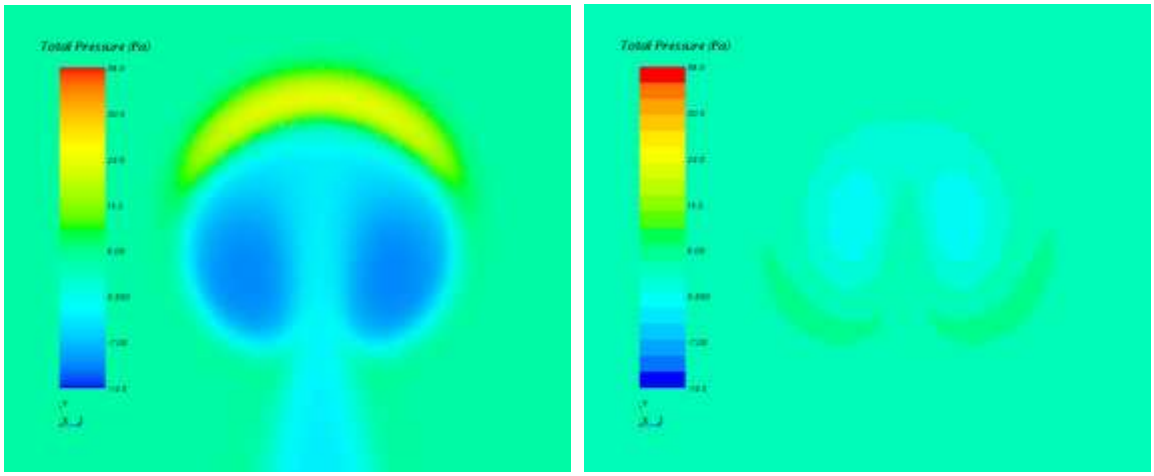

FIGURE 47. Total pressure for r=2 with L/D=0, left x/D=1, right x/D=5.

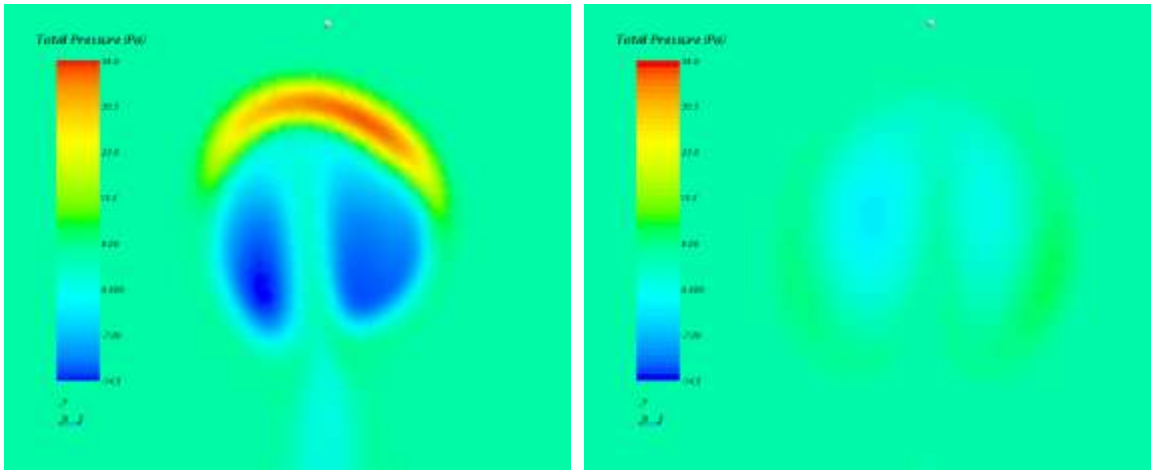

FIGURE 48. Total pressure for r=2 with L/D=2, left x/D=1, right x/D=5.

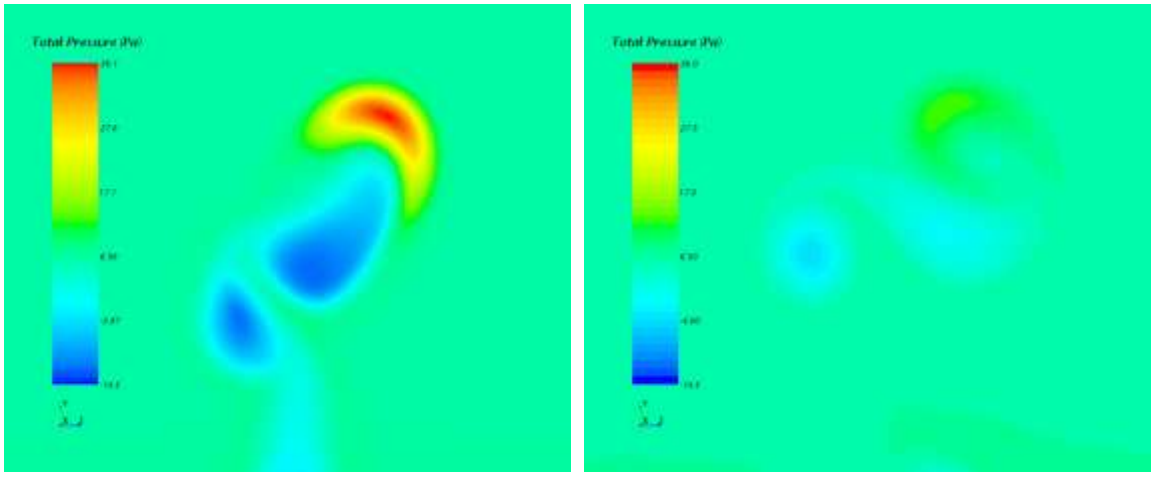

FIGURE 49. Total pressure for r=2 with L/D=11.25, left x/D=1, right x/D=5.

3.6 r=5

3.6.1 Velocity Vector

Unlike the results for r=2, there is no destruction of the CVP at r=5 but an asymmetrical counter rotating pair is formed for both coil inserts. Although the swirl number remained at 0.23 for L/D=11.25 the CVP did not breakdown as in r=2. When L/D=2, the formation of a CVP is not clearly seen at the jets exit. The delay in formation of CVP could be attributed to the constriction (narrowing of the internal diameter) for which it creates a higher momentum in the y-axis and hindering the shear layer vortices. Swirl number for L/D=2 decreases from 0.08 at r=2 to 0.06. The decrease in swirl strength could be due to the increased jet velocity, reducing sufficient time required for swirl formation. For jets with coil inserts, the vortex on the right hand side is bigger than the one on the left side.

3.6.2 Turbulent Kinetic Energy

With coil insert, TKE is increased significantly. Initially, the coil-inserted jet with L/D=11.25 had the greatest increase of nearly 150% while the coil-inserted jet with L/D=2 had about 40% increase when compared to a smooth jet. With L/D=11.25, TKE kept a higher value throughout the entire flow domain whereas the jet with L/D=2 and the smooth jet, had nearly the same value through the remaining flow domain. The significant increase in TKE for the jet with L/D=11.25 results in the highest mixing enhancement as compared to the jet with L/D=2 and the smooth jet which also results in reduced jet penetration. Results correlate to the CVP width increased that is seen with L/D=11.25 than that of L/D=2, indicating greater interaction between the jet and the crossflow.

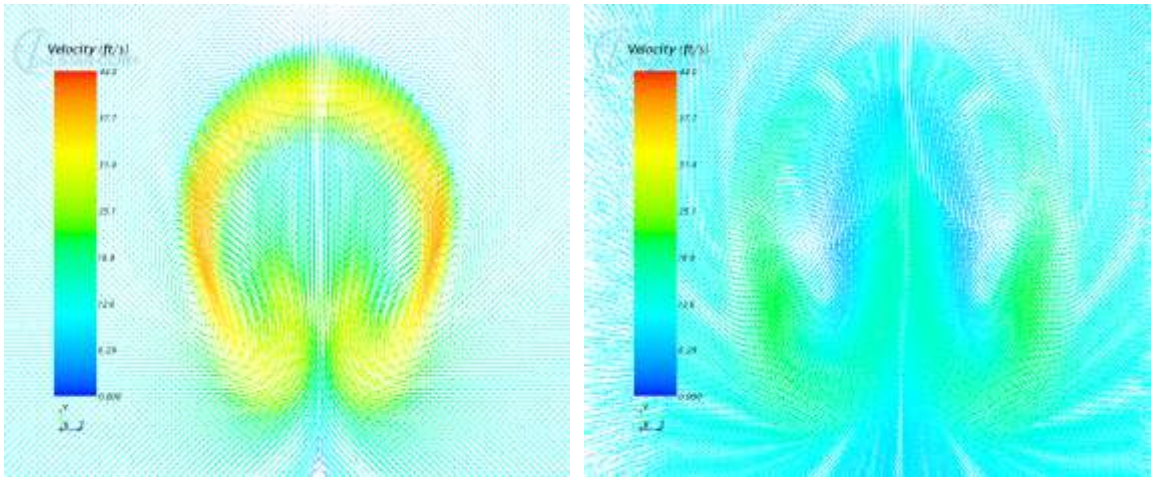

FIGURE 50. Velocity vector for r=5 with L/D=0, left x/D=1, right x/D=5.

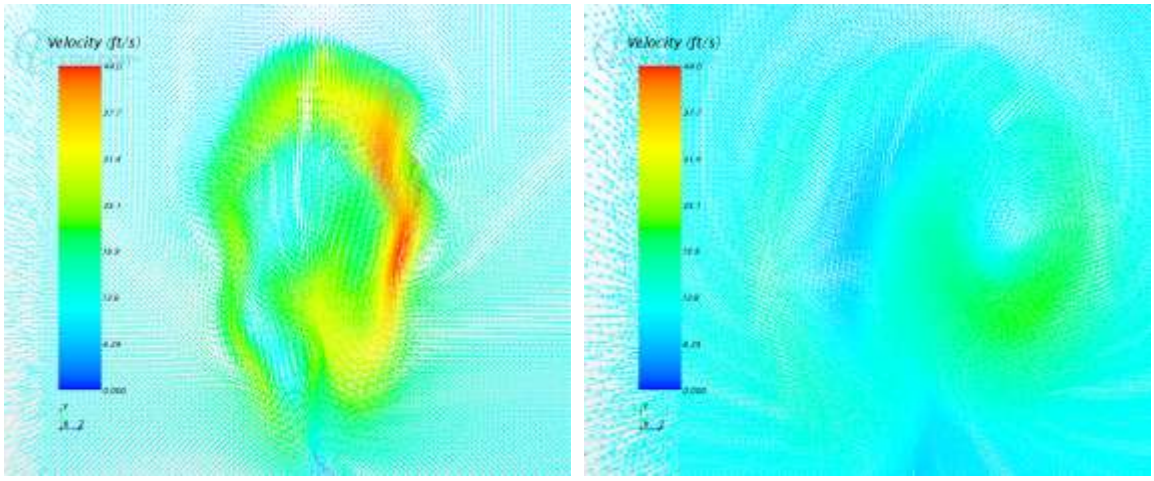

FIGURE 51. Velocity vector for r=5 with L/D=2, left x/D=1, right x/D=5.

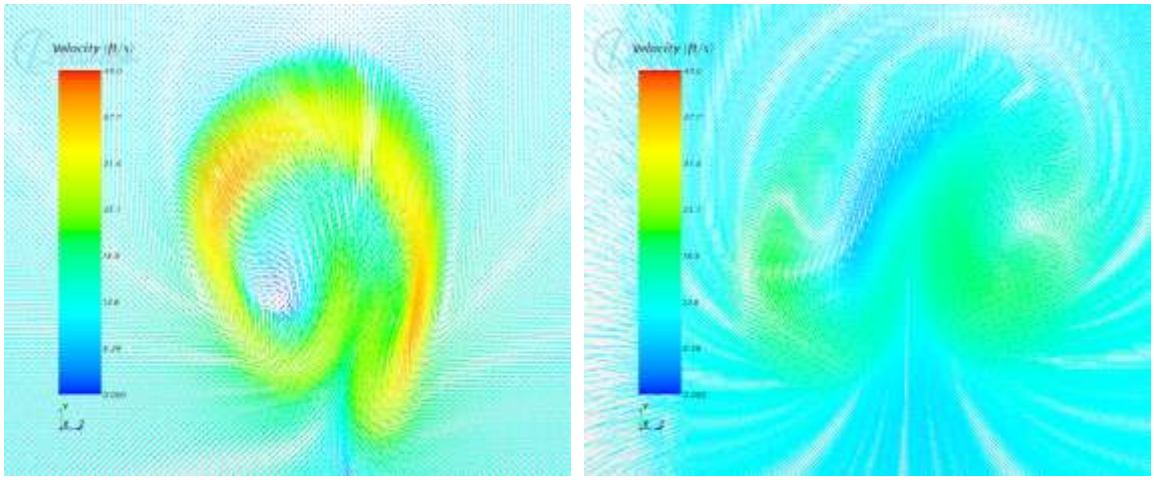

FIGURE 52. Velocity vector for r=5 with L/D=11.25, left x/D=1, right x/D=5.

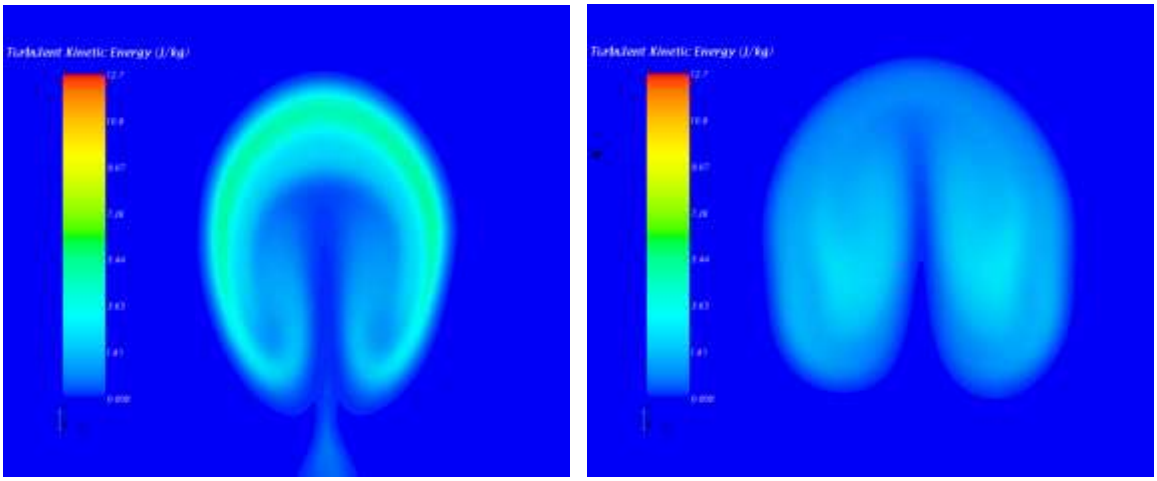

FIGURE 53. TKE for r=5 with L/D=0, left x/D=1, right x/D=5.

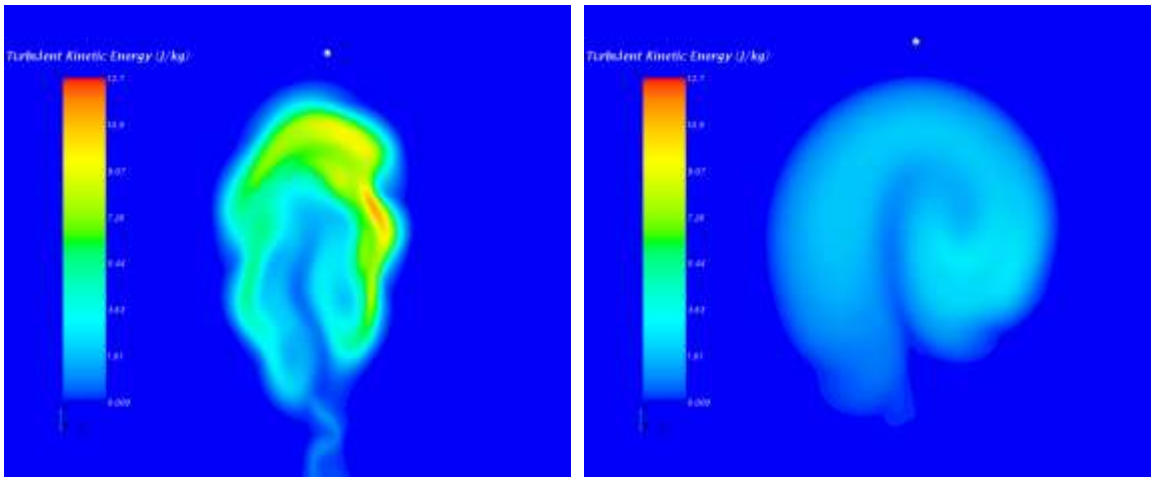

FIGURE 54. TKE for r=5 with L/D=2, left x/D=1, right x/D=5.

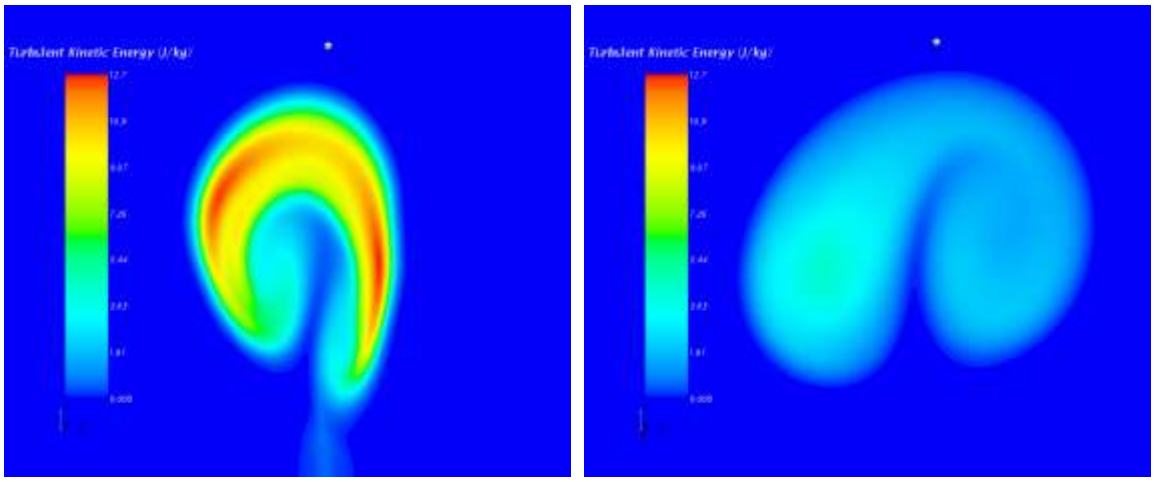

FIGURE 55. TKE for r=5 with L/D=11.25, left x/D=1, right x/D=5.

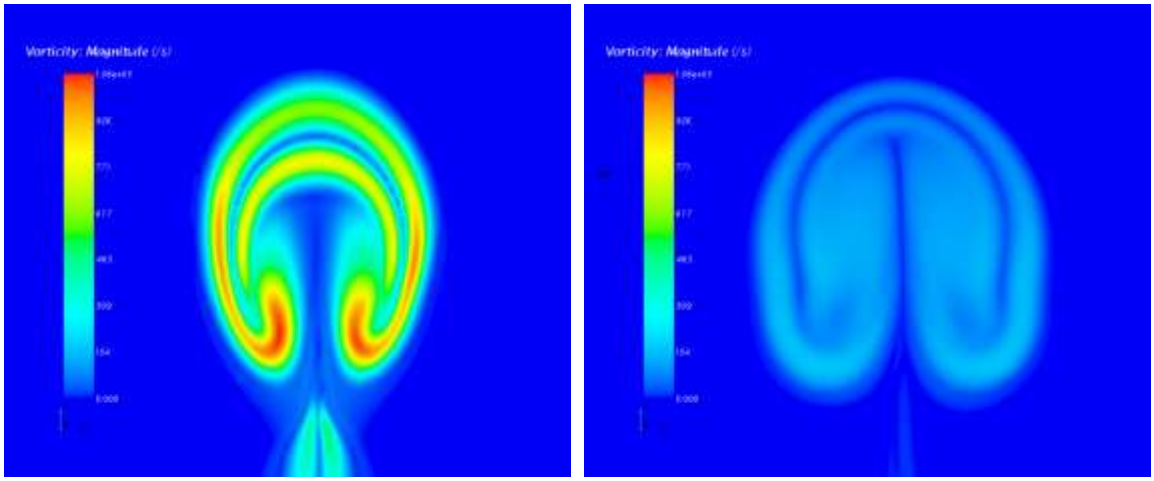

FIGURE 56. Vorticity for r=5 with L/D=0, left x/D=1, right x/D=5.

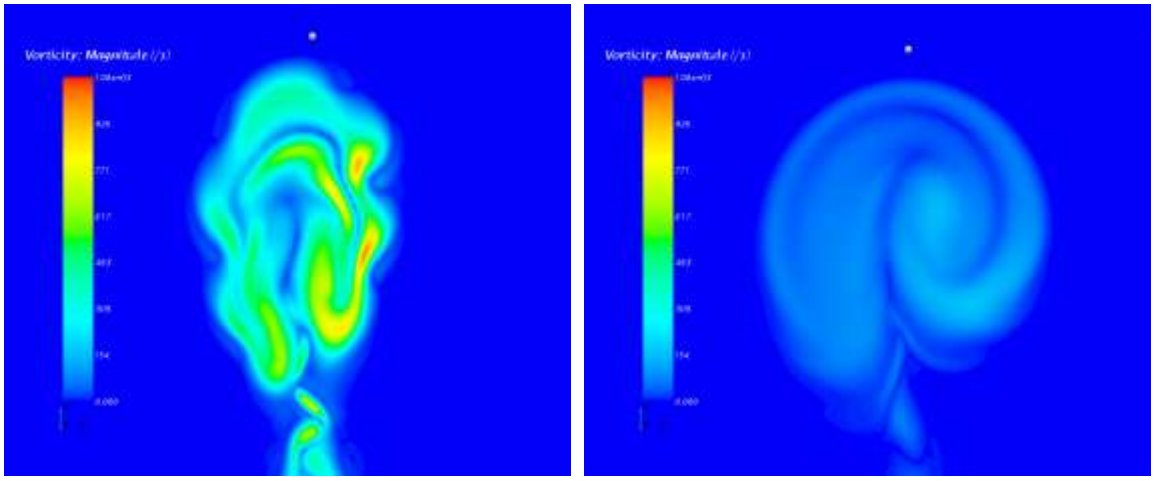

FIGURE 57. Vorticity for r=5 with L/D=2, left x/D=1, right x/D=5.

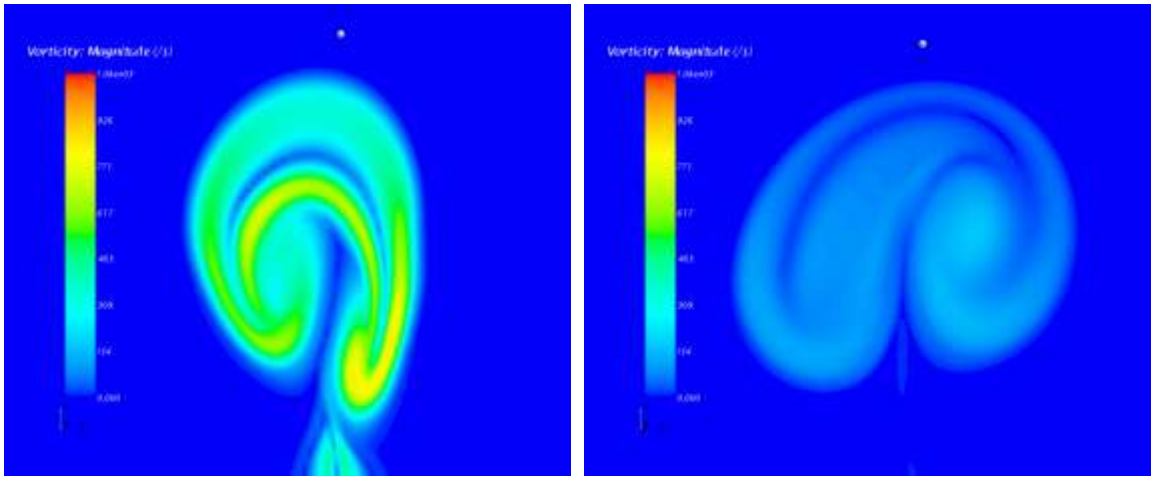

FIGURE 58. Vorticity for r=5 with L/D=11.25, left x/D=1, right x/D=5.

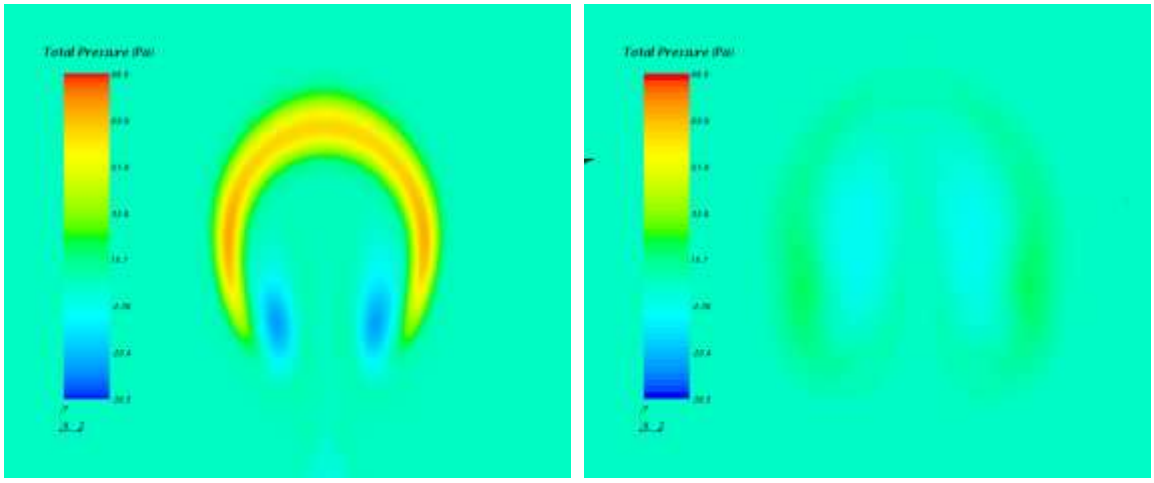

FIGURE 59. Total pressure for r=5 with L/D=0, left x/D=1, right x/D=5.

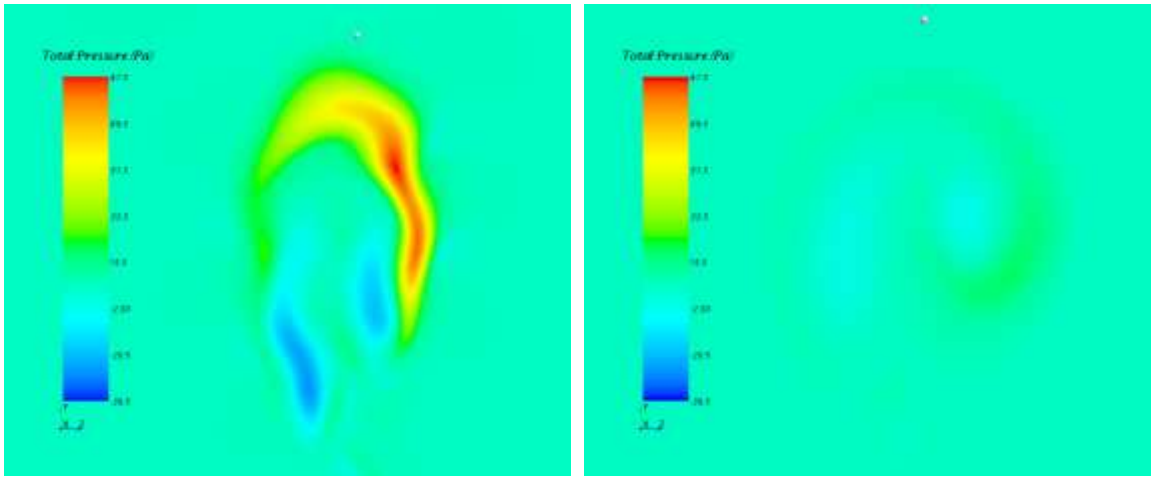

FIGURE 60. Total pressure for r=5 with L/D=2, left x/D=1, right x/D=5.

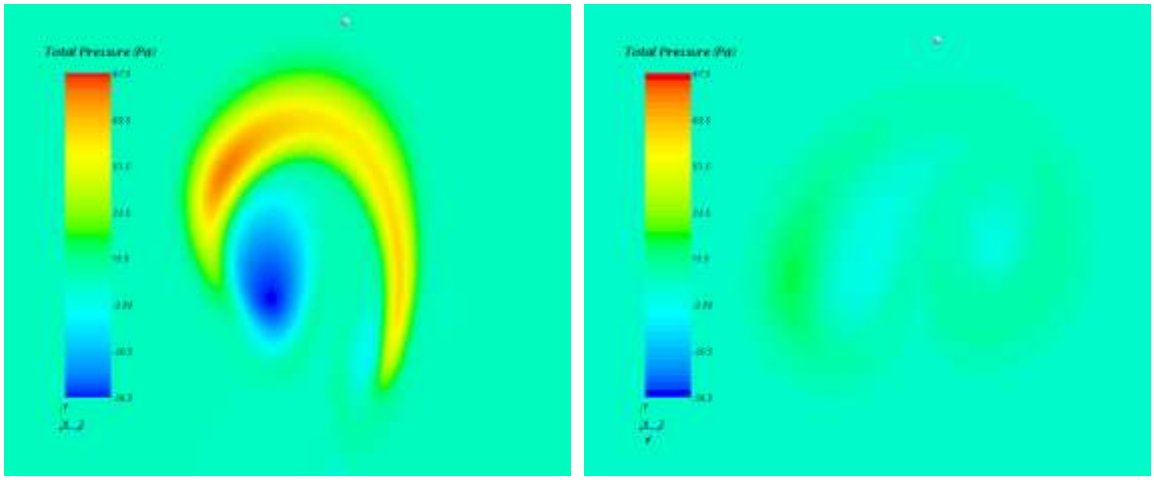

FIGURE 61. Total pressure for r=5 with L/D=11.25, left x/D=1, right x/D=5.

3.6.3 Vorticity

The coil-inserted jets had reduced vortices, when compared to the corresponding results for the smooth tube. Higher TKE results in increased mixing and reduced vortices generation, especially at downstream locations. The vortices contours for the coil-inserted jets are not symmetric with a stronger vortex seen on the right hand side as compared to the left hand side, which could be as the result of the right vortex and swirl generated from the coil insert having the same flow direction.

3.6.4 Total Pressure

Total pressure is highest around the CVP and is due to high entrainment and lower velocity. The low pressure is due to existence of the vortex core, which is mostly due to the low static pressure. Greatest pressure difference with the three cases is seen only at x/D=1 and further downstream the differences in pressure disappear and the results for all three jets are nearly the same.

3.7 Jet Trajectory

One of the objectives of the jet in crossflow simulations was to study the effects of the coil insert had on the jet trajectory. Jet trajectories were found using the locations of the highest axial velocity in the crossflow direction. Jet trajectories are expressed in the form of a power law equation where the vertical and axial distances are usually scaled by D, rD, or r^2D. Here D is the inside diameter of the tube. Although using r^2D scaling has shown to be more accurate in defining the jets trajectory by having jet trajectories collapse, scaling with rD is used in the following results due to the fact that it captures the current results more accurately [13]. Figures 62-64 show the jet trajectories with fitted power law.

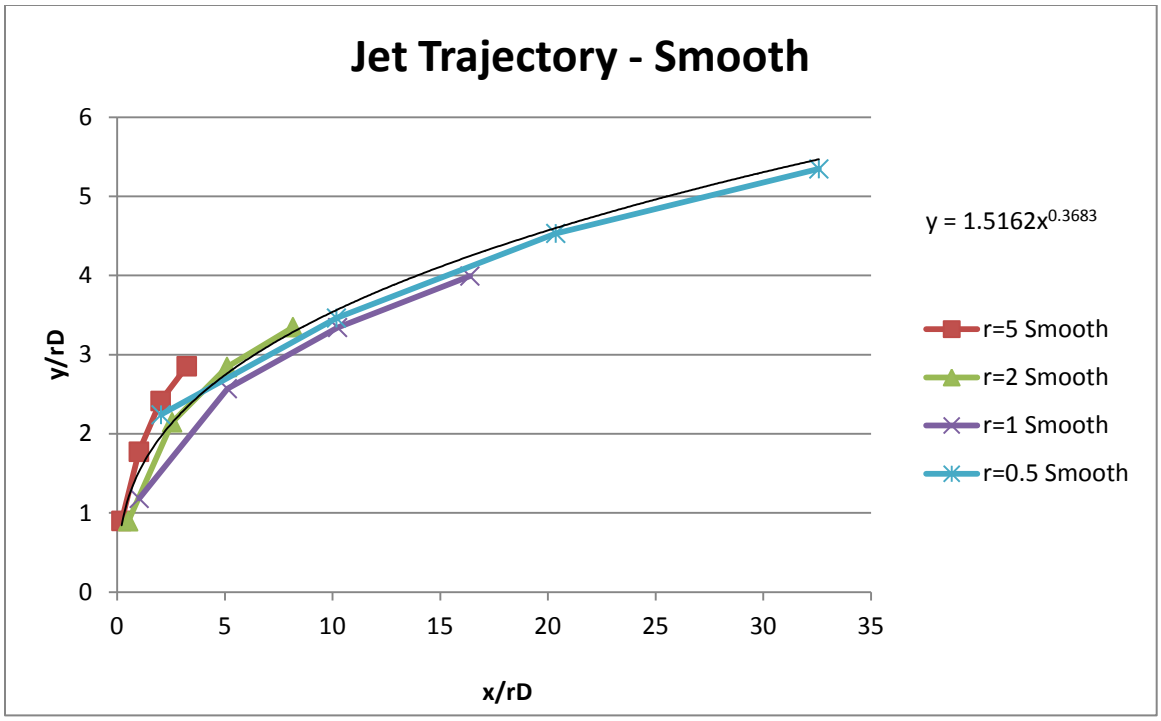

FIGURE 62. Jet trajectories of r = 0.5, 1, 2, 5 with L/D=0.

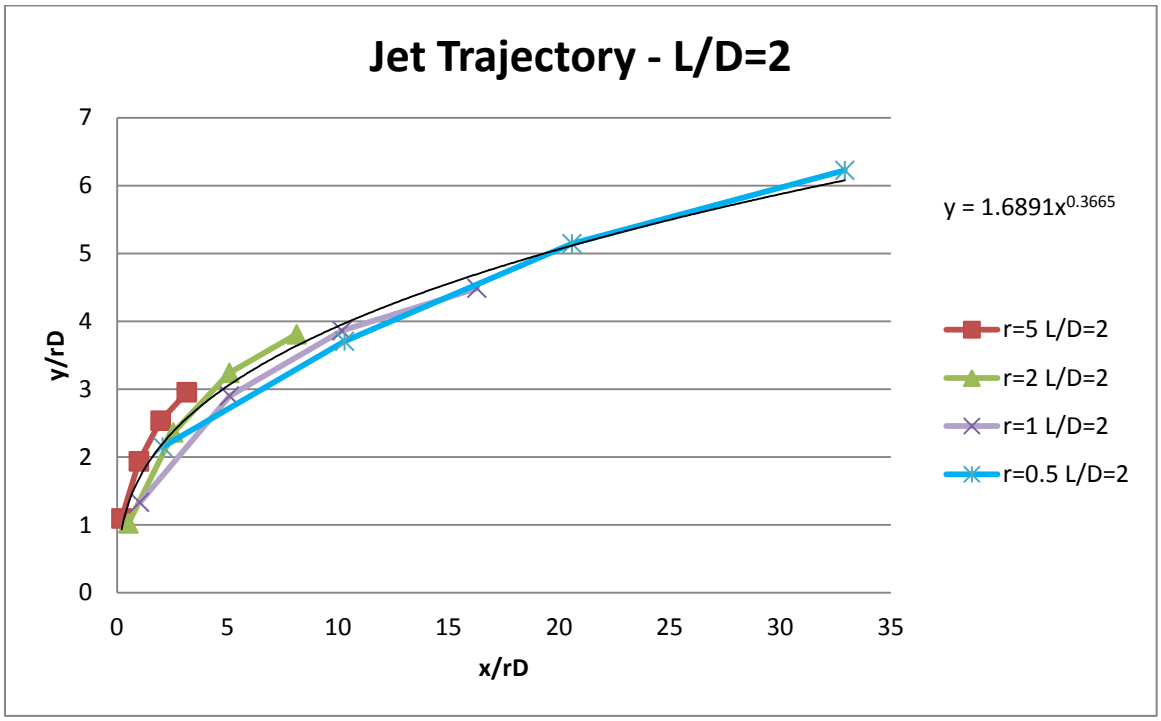

FIGURE 63. Jet trajectories of r = 0.5, 1, 2, 5 with L/D=2.

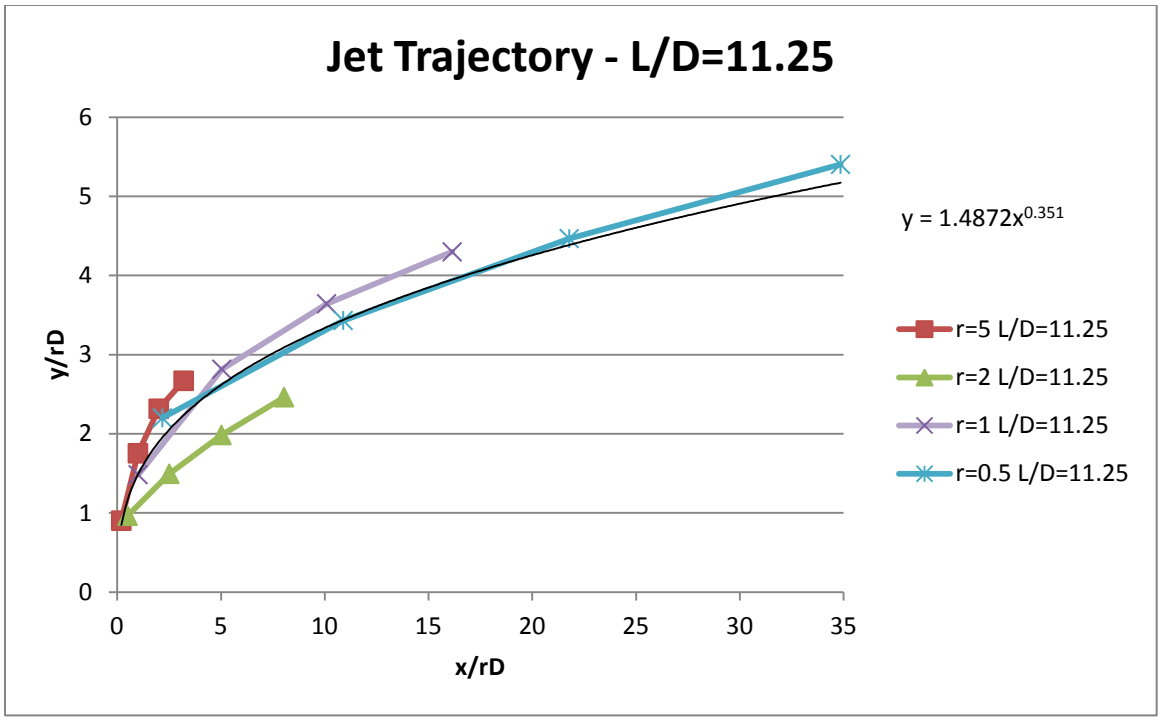

FIGURE 64. Jet trajectories of r = 0.5, 1, 2, 5 with L/D=11.25.

It can be concluded that with a coil insert of L/D=11.25 the jet penetration has decreased, in accordance with Kalfas et al. [11]. It is to note that jet trajectory did not decrease as much as the results from Kalfas et al. [11] show which could be due to the contraction that the coil impose on the flow creating a nozzle effect and preventing entrainment until further distance downstream. Since the pipe velocity inlets were the same for all three cases, it is safe to say that they had the same initial momentums and thus, considering conservation of momentum, the variation in turbulent kinetic energy of the flow in the near field has a direct impact on the jets trajectories.

For the case with L/D=2, initial jet penetration is seen to slightly increase rather than decrease as compared with the jet with L/D=11.25. The initial gain in penetration is the

direct effect of the shorter coil, acting more as a nozzle than a "swirler," giving the jet a higher throw.

The initial higher penetration of the jets correlate with decrease in TKE for r=0.5 and for r=1. For r equal to 2 and 5, the jet trajectory decreases as TKE increases. For a coil insert of L/D=2 the jet trajectory initially maintain a higher value than that of a smooth orifice due to the higher throw seen before the jet tilts. On the contrary, L/D=11.25 where jet trajectory decreases significantly reaching a lower value to that of non coil insert. An important reminder is: L/D=11.25 had a greater increase value in TKE than that of L/D=2 explaining the decrease in jet throw an intern a decrease in jet trajectory and increase in CVP width.

Table 4 demonstrates the three different power equations fitted through all four velocity ratios used in all three cases and displays the overall effect of the coil insert on the jet trajectory, $y^{*}= Ax^{*m}$.

TABLE 4. Fitted Power Law for All Velocity Ratios Non-Dimensionalized by rD

	L/D=0	L/D=2	L/D=11.25
A	1.5162	1.6891	1.4872
m	0.3683	0.3665	0.3510

As mentioned before, the jet with L/D=2 initially penetrate the crossflow further where as the jet with L/D=11.25 has reduced jet penetration from the jet exit. The significance of using a power law trend line, $y^{*}= Ax^{*m}$, is that it can be converted to a log-log graph and intern creates a linear line, allowing for a better understanding of the jets trajectory. The variable A becomes the location of cross section in the y-axis, identifying the virtual location of the jet and m becomes the slope of the line indicating

the rate of jet penetration, when the power equation is converted into a log-log form. A log-log form equation shows that even though L/D=2 has a higher throw, the flow from the smooth jet will eventually surpass it in the far field. Furthermore, the jet with L/D=11.25 maintains a lower rate of penetration throughout the flow. In summary, an increase in turbulent kinetic energy has a direct impact on the jets entrainment.

CHAPTER 4

CONCLUSIONS

The initial effects of inserting rigid coils, of L/D=2 and L/D=11.25, inside a pipe jet issuing into a crossflow were examined numerically. The CD-Adapco's computational fluid dynamics program, StarCCM+, was used to carry out the analyses. A constant crossflow velocity of 10 ft/s was held with alterations in jet inlet velocity to obtain the different velocity ratios, r, of 0.5, 1, 2, and 5 while maintaining jet diameter at 2 inches. Reynolds numbers based on the mean jet velocity ranged from 4600 to 49000 for the plane pipe, for the coil insert with L/D=2 ranged from 4800 to 49200, and for the coil insert with L/D=11.25 values were 4900 to 49300. Reynolds number increased due to the reduction in inside diameter with the coil inserts, resulting in higher jet mean velocity. The crossflow Reynolds number based on pipe diameter was Re_D=9884 and per unit length was 4942.

The two different coil inserts were used to compare results to that of the smooth tube in planes perpendicular to the axial flow at stream wise locations of x/D=1, 5, 10, and 16 with detailed results provided at x/D=1 and x/D=5. To allow for fully developed flow the length of the orifice was of 12D for L/D=0, the same length was used for the pipe with the coil insert with L/D=11.25 but for the pipe with the coil insert of L/D=2 the length was increased to 20D to allow a fully developed flow before reaching the coil.

Results show that depending on the coil length, it acts as a swirl generator, or a turbulator. Swirl intensity increases as the velocity ratio increases but it is important to

note that the shorter coil insert will produce a weaker swirl number and behaves more like a turbulator than a swirl generator. Furthermore, a shorter coil of L/D=2 has a greater nozzle effect as the jet throw increases.

The jet with a coil insert of L/D=11.25 tends to carry a higher TKE in the near field whereas the one with L/D=2 carried a higher TKE in the far field when comparing the results from these two jets. The jet with L/D=2 has a higher jet trajectory than that with L/D=11.25 at all velocity ratios.

The width of the CVP was seen to be hindered with the addition of the coil insert for r=0.5 and r=1. When r=2 and 5, the width of the CVP had increase with the coil with L/D=11.25 having a greater increase than that of the coil with L/D=2, allowing for greater crossflow entrainment and mixing.

For r=2, the destruction of the CVP has occurred and could be a direct effect that the flow at the jet exit is eccentric to the right of the flow, $z > 0$. Also visible; at x/D=16 the formation of an asymmetric CVP.

For $r \geq 2$, at the jet outlets, flows with coil inserts had a significant increase in TKE, when compared with the corresponding results for the smooth pipe which also results in reduced jet penetration. Jet trajectory did not decrease further than L/D=0 with L/D=2, due to the higher throw the jet has before tilting into crossflow direction, even though there was a slight increase in TKE. But from the power law trajectory equations, flow from the smooth pipe would ultimately carry a higher penetration.

Jet trajectory equations, when all velocity ratios are taken into account, showed that the coil-inserted jet with L/D=2 had the highest initial entrainment and the one with L/D=11.25 had the lowest. Results showed that even though the jet with L/D=2 had

higher initial entrainment; the flow with pipe without coil had higher slope meaning the overall entrainment would be higher beyond x/D=16.

Mixing and jet penetration were shown to be a trade off of each other for different velocity ratios. Greater mixing in the near field leads to lower jet penetration and greater jet penetration associated with reduced entrainment in the near field. The pipe jet without coil insert would ultimately carry the highest jet trajectory.

For coil-inserted jets, higher velocity ratios, $r \geq 2$, showed to have higher mixing enhancement and results for r=0.5 showed to have reduced mixing.

APPENDIX

ISO-SURFACE FIGURES

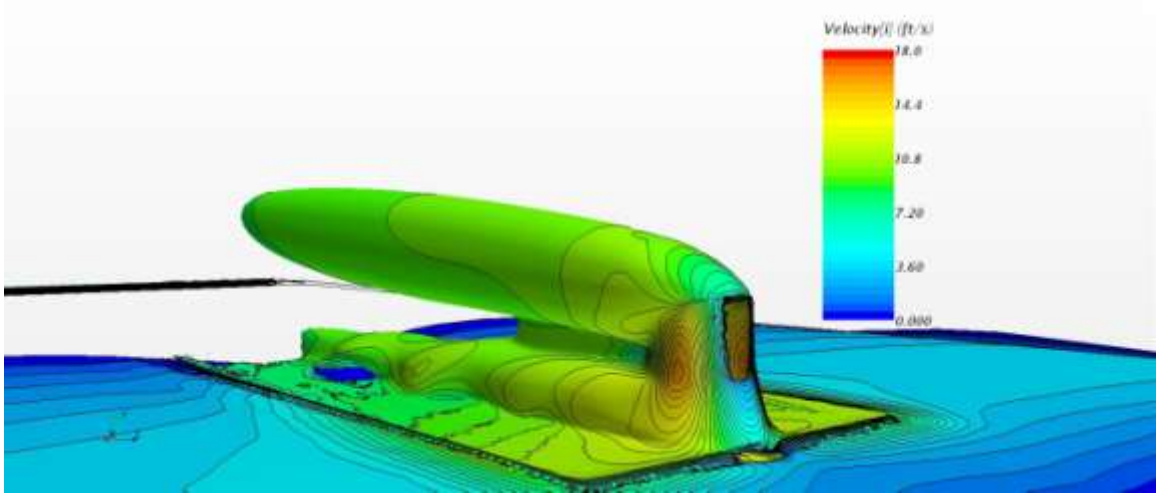

FIGURE 65. Iso-surface from TKE results for axial velocity for r = 0.5 with L/D = 0.

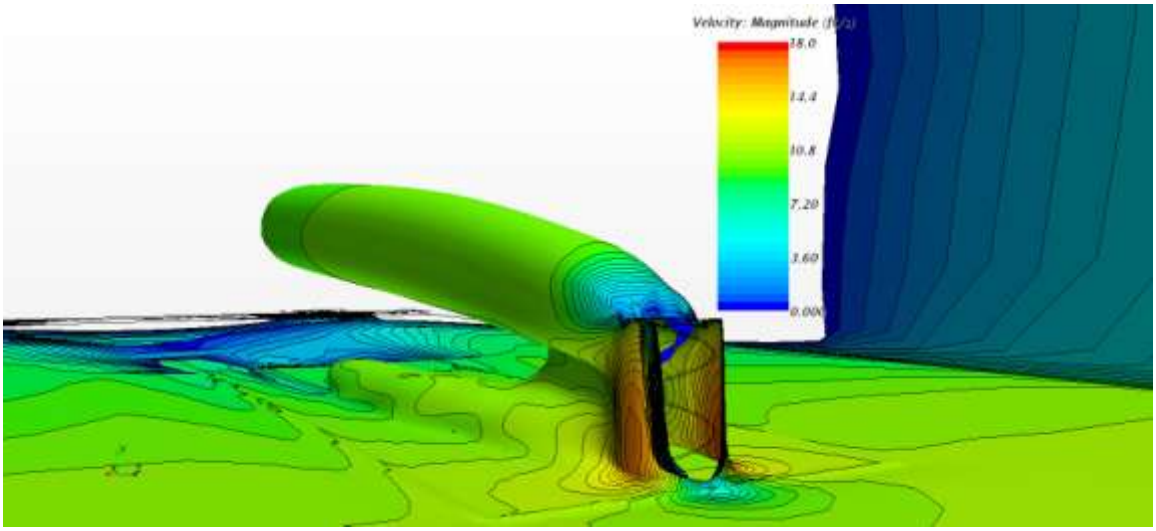

FIGURE 66. Iso-surface from TKE results for axial velocity for r = 0.5 with L/D = 2.

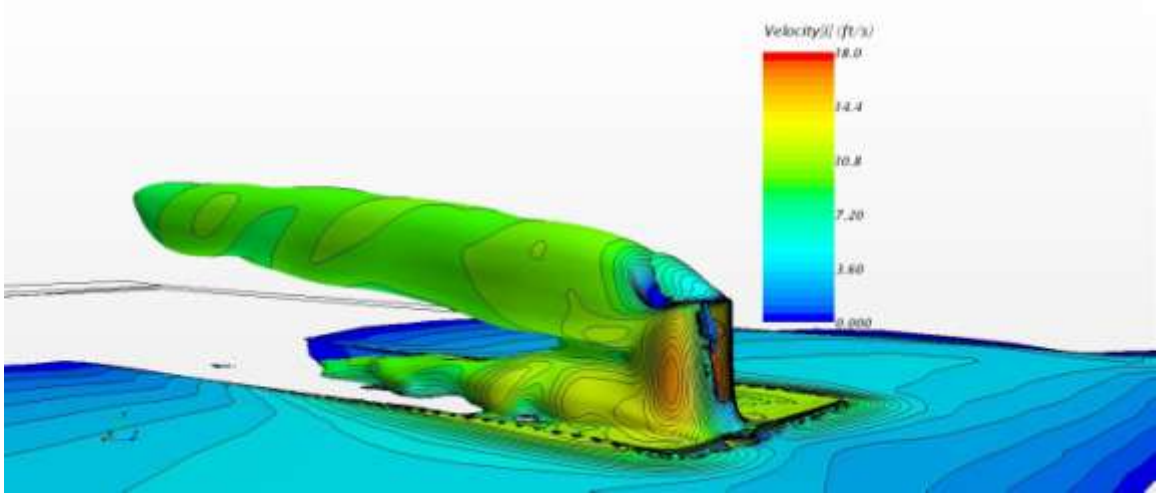

FIGURE 67. Iso-surface from TKE results for axial velocity for r = 0.5 with L/D = 11.25.

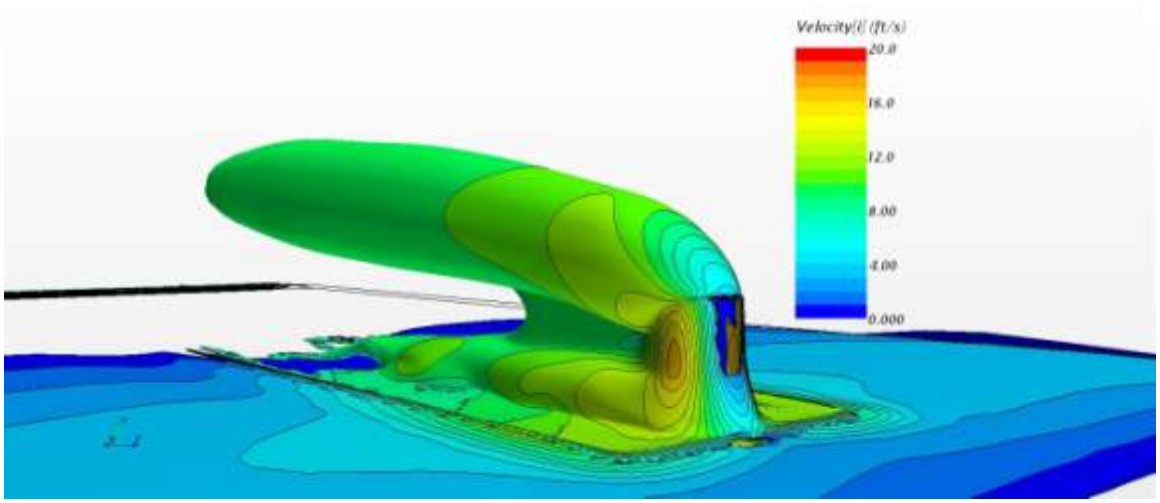

FIGURE 68. Iso-surface from TKE results for axial velocity for r = 1 with L/D = 0.

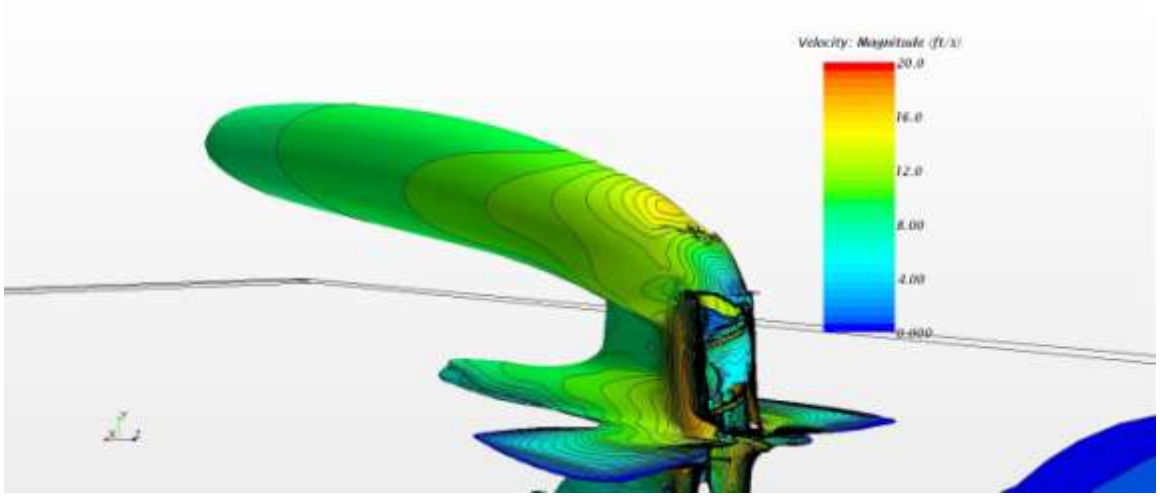

FIGURE 69. Iso-surface from TKE results for axial velocity for r = 1 with L/D = 2.

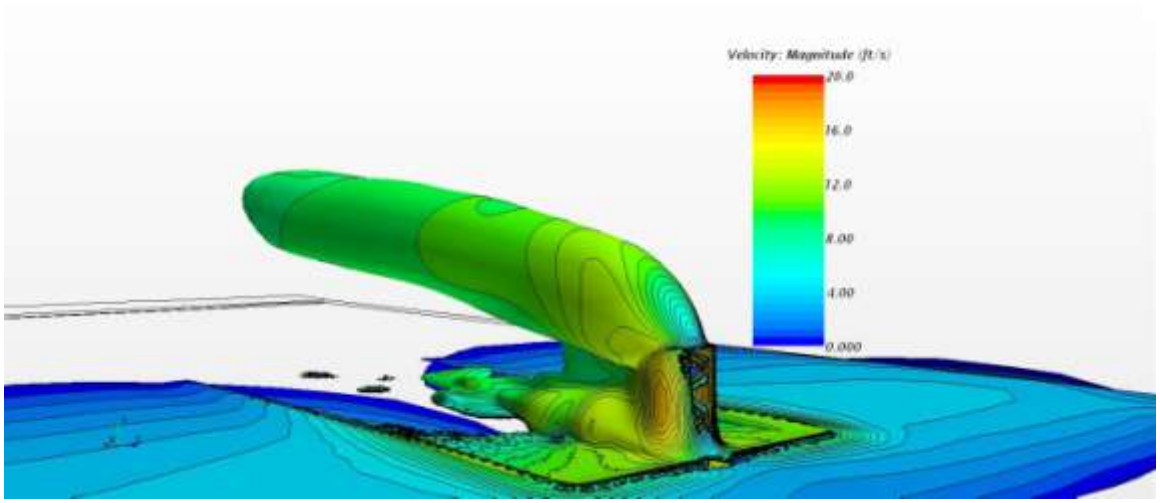

FIGURE 70. Iso-surface from TKE results for axial velocity for r = 1 with L/D = 11.25.

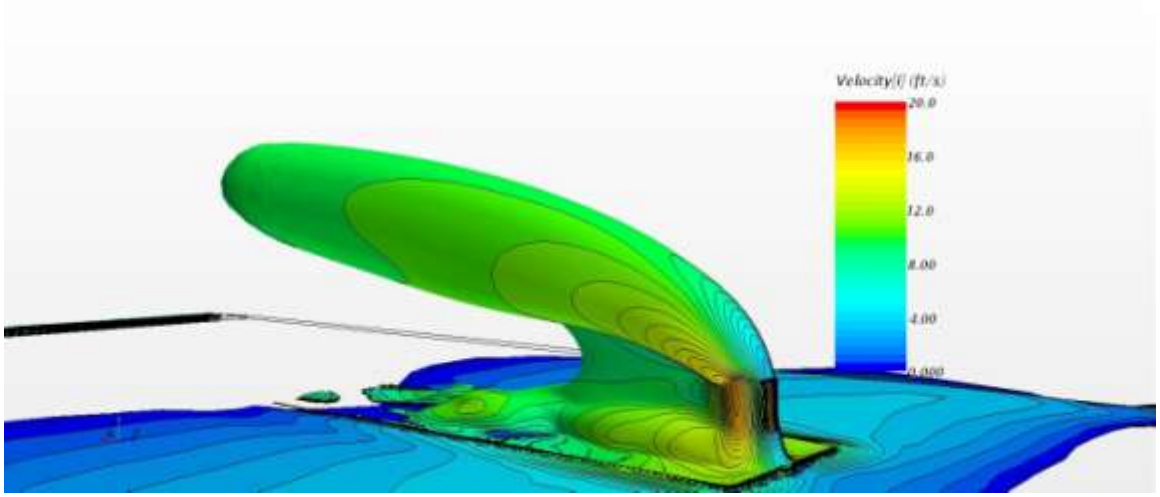

FIGURE 71. Iso-surface from TKE results for axial velocity for r = 2 with L/D = 0.

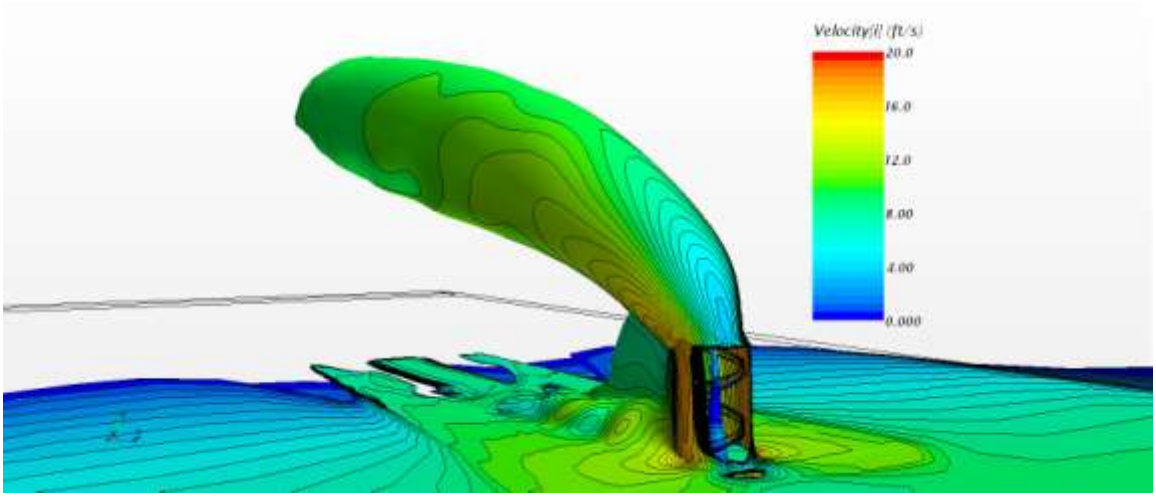

FIGURE 72. Iso-surface from TKE results for axial velocity for r = 2 with L/D = 2.

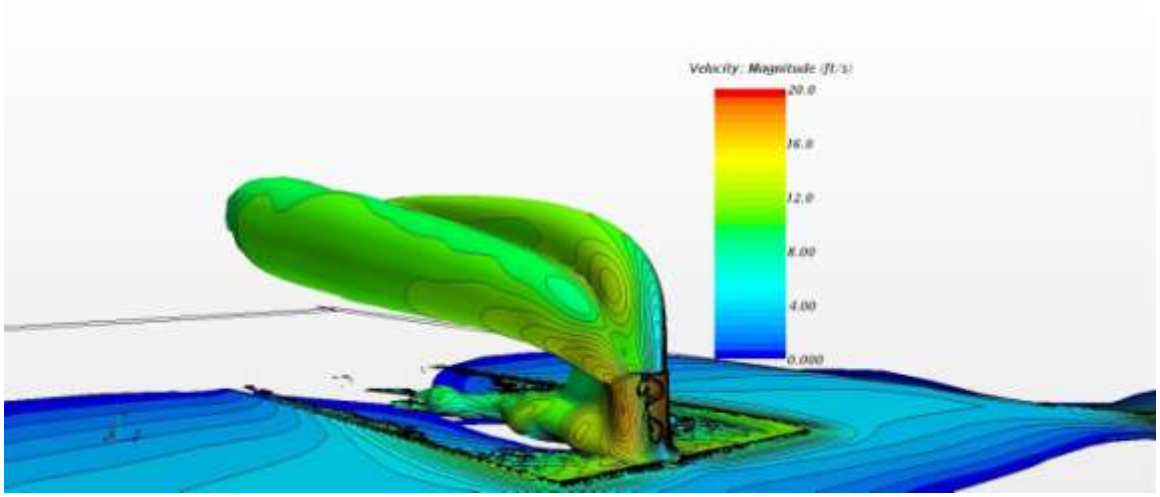

FIGURE 73. Iso-surface from TKE results for axial velocity for r = 2 with L/D = 11.25.

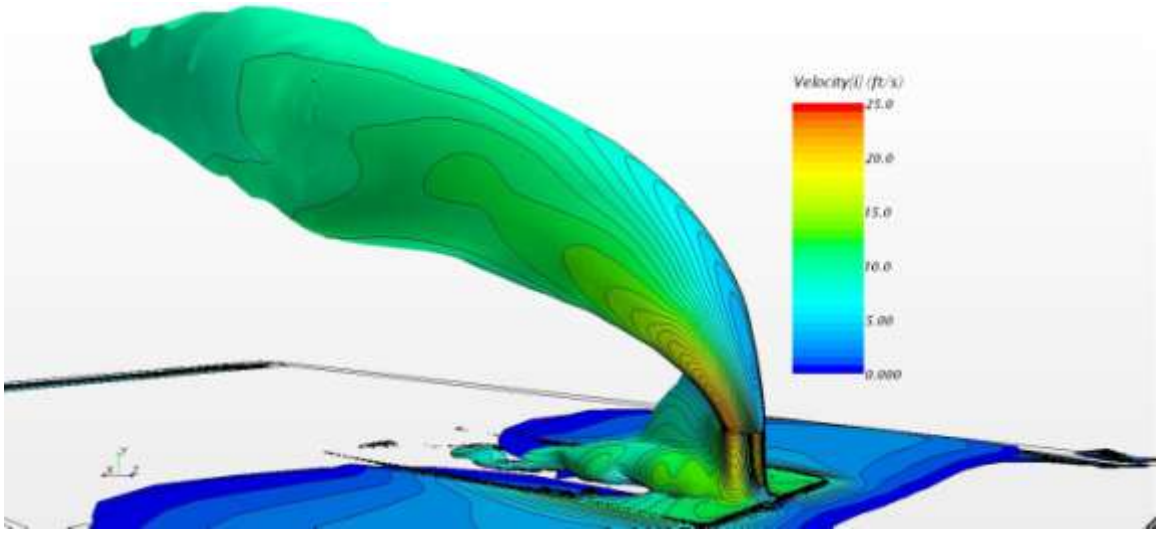

FIGURE 74. Iso-surface from TKE results for axial velocity for r = 5 with L/D = 0.

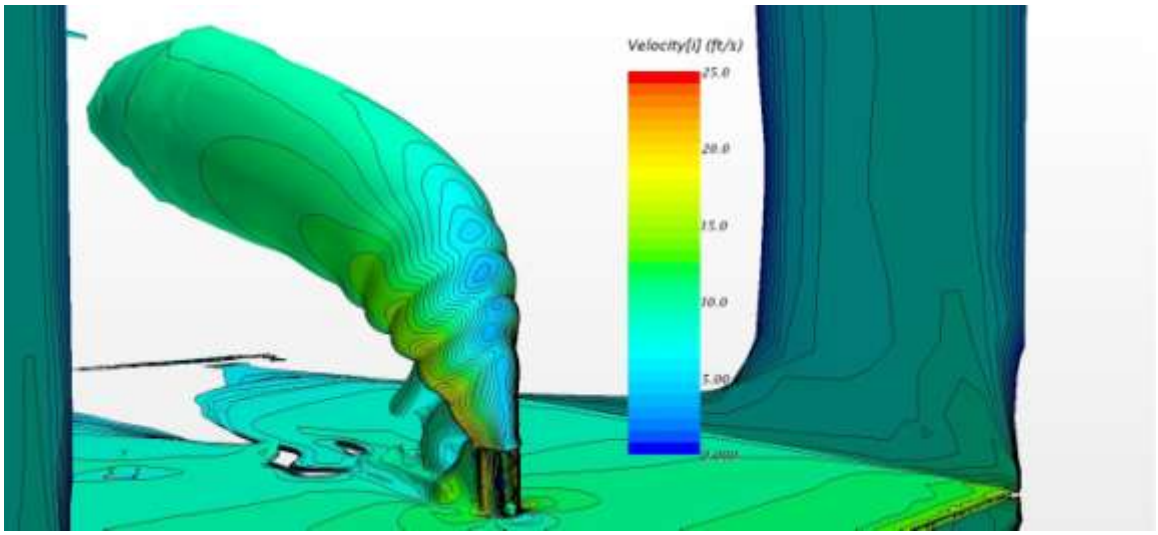

FIGURE 75. Iso-surface from TKE results for axial velocity for r = 5 with L/D = 2.

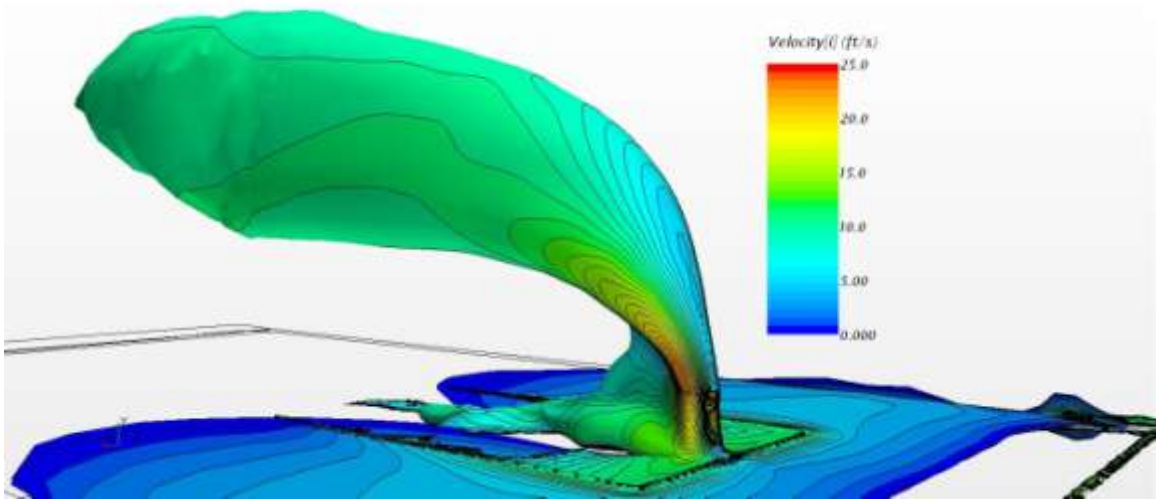

FIGURE 76. Iso-surface from TKE results for axial velocity for r = 5 with L/D = 11.25.

REFERENCES

REFERENCES

[1] Andreopoulos, J., and Rodi, W., 1984, “Experimental Investigation of Jet in Cross Flow,” Journal of Fluid Mech., 138, pp. 93-127.

[2] Smith, S.H., and Mungal, M. G., 1998, “Mixing Structure and Scaling of the Jet in Cross Flow,” Journal of Fluid, 357, pp. 83-122.

[3] Fric, T.F., and Roshko, A., 1994, “Vertical Structure in the Wake of a Transverse Jet”, Journal of Fluid Mech., 279, p. 1-47.

[4] Eiff, O. S., Kawall, J. G., and Keffer, J. F., 1994, “Lock-in of Vortices in the Wake of an Elevated Round Turbulent Jet in Cross Flow,” Exps. Fluids, 19, pp. 203- 213.

[5] Habli, S., Mhiri, H., and Said, N. M., 2007, “Flow Field Measurements in a Crossflowing Elevated Jet,” J. Fluids Engineering, 129, pp. 551-562.

[6] Almoukdad, M. Y., Hoang, H. T., and Rahai, H.R., 2004, “The Distortion of a Round Jet by Coil Inserts of Various Lengths,” Applied Thermal Engineering, 24, pp. 351-358.

[7] Feyedelem, M. S., and Sarpkaya, T., 1998, "Free- and Near-Free-Surface Swirling Turbulent Jets," AIAA Journal, 36, 3, pp. 359-364.

[8] Kalfas, A. I., Kazakos, C., Ott, P., Terzis, A., and Zachos, P. K., 2012, “Swirl Jets in Crossflow at Low Velocity Ratios,” Journal of Mechanics Engineering and Automation, 2, 4, pp. 256-266.

[9] Kalfas, A. I., Pilidis, P., and Zachos, P. K., “Effects of Swirl Velocities from Fan Assemblies Mounted on Lifting Surfaces,” Journal of Engineering Gas Turbines Power, 133, 2011, doi: 10.115/1.4002099.

[10] Pratte, B.D., and Baines, W.D., 1967, “Profiles of the Round Turbulent Jet in a Cross Flow,” Journal of Hydronaut, Div. ASCE, 92, pp. 53-64.

[11] Dai, Z., Hsieh, S., and Mongia, H. C., “Modeling of Jets in Cross Flow with RANS and LES Part 1: Momentum Transport for Low R w/RANS,” 43nd AIAA Aerospace Sciences Meeting and Exhibit, 2005.

[12] Orrala, C., and Rahai, H. R., 2004 “Experimental Investigations of Two Side-by-Side Jets in a Cross Flow,” 42nd AIAA Aerospace Sciences Meeting and Exhibit.

[13] Baines, W.D., and Keffer, J.K., 1963, “The Round Turbulent Jet in Cross-flow,” Journal of Fluid Mechanics., 15, pp. 481-496.

[14] Eskinazi, S., Moussa, Z. M., and Trischka, John W., 1977, “The Near Field in the Mixing of a Round Jet with a Cross-Stream,” Journal of Fluid Mechanics, 80, pp. 49-80.

[15] Farokhi, S., Rice, E. J., and Taghavi, R., 1989, "Effect of Initial Swirl Distribution on the Evolution of a Turbulent Jet," AIAA Journal, 27, 6, pp. 700-706.

[16] Lim, T. T., Kelso, R. M., and Perry, A. E., 1996, “An Experiment Study of Round Jets in Cross-Flow,” Journal of Fluid Mechanics, 306, pp. 111-114.

[17] Mahesh, K., 2013, “The Interaction of Jets with Crossflow,” Annual Review of Fluid Mechanics, 45, pp. 379-407.

[18] Meyer, K. E., Cavar, D., 2012, “LES of Turbulent Jet in Cross-Flow: Part 1 – A Numerical Validation Study,” International Journal of Heat and Fluid Flow, 36, pp. 18-34.

[19] Saha, A. K., Yaragani, C. B., 2012, “Three-Dimensional Numerical Study of Jet-in-Crossflow characteristics at Low Reynolds Number,” Heat Mass Transfer, 48(2), pp. 391-411.